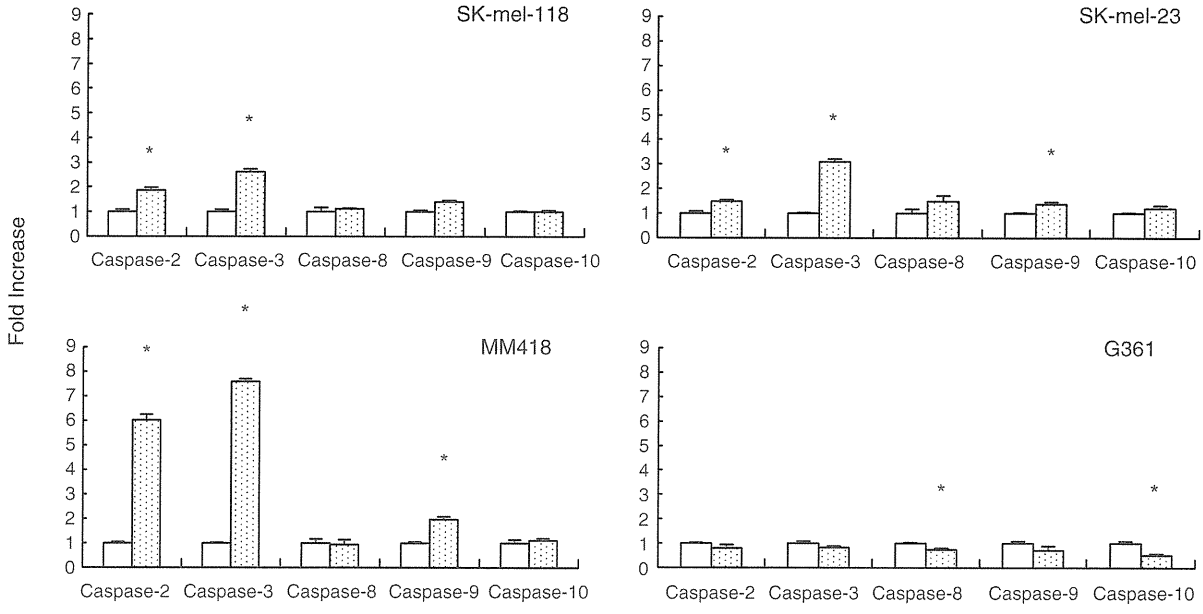


FIG. 3. Caspase assay after treatment with interferon (IFN)-β. Cells were plated on 10-cm dishes with $2 \times 10^4$ cells/mL. The cell lines were treated with 1,000 IU/mL IFN-β in triplicate. After 48 h, cells were harvested and caspase activity was assessed by caspase fluorometric assay as described in the manufacturer's protocol. The caspase activity is expressed as the fold increase compared with the untreated cells. The results are expressed as relative values (mean ± S.D.) to untreated controls. Untreated: empty column, IFN-β: dotted column. *Significant difference ($P < 0.01$) from the value in the untreated control.

blotting was not enough to detect the active caspase fragment in these IFN-β-treated cells. The levels of procaspase-2 and -3 were not up-regulated by treatment with IFN-β in all cell lines (data not shown). The IFN-β-induced apoptosis in MM418, SK-mel-23, and SK-mel-118 was significantly suppressed by the addition of inhibitor for caspase-2 or caspase-3, and these inhibitors showed equivalent anti-apoptotic effect against IFN-β-induced apoptosis. However, the inhibitors for both caspase-8 and caspase-9 did not show any anti-apoptotic effect by IFN-β (Fig. 5). These results indicated that caspase-2 and caspase-3 induced had critical role on IFN-β-induced apoptosis as an initiator and an effector for caspases, respectively.

### *Exogenous TRAIL caused apoptosis in melanoma cells*

To elucidate the mechanism of IFN resistance in melanoma cells, we treated the 4 melanoma cell lines by adding exogenous apoptosis-inducing ligands (Fig. 4). When G361 and SK-mel-118 were treated with TRAIL, TNF-α, or an anti-Fas (CD95) antibody, TRAIL significantly reduced their cell viability. The anti-Fas (CD95) antibody also reduced the cell viability of SK-mel-118. The cell viabilities of SK-mel-23 and MM418 were not influenced with treatment of exogenous apoptosis-inducing ligands (Fig. 6). We also examined the effect of anti-TRAIL antibodies on the IFN-β-induced apoptosis. Anti-TRAIL antibody slightly suppressed IFN-β-induced apoptosis but did not show significant anti-apoptotic effect induced by IFN-β in SK-mel-118 and SK-mel-23. IFN-β-induced apoptosis was not suppressed by anti-TRAIL antibody in MM418 (data not shown). Furthermore, the cell viability of those tested cells was assessed after treatment with IFN-β, followed by apoptosis-inducing ligands treatment. IFN-β pretreatment followed by TRAIL stimulation significantly reduced the cell viability compared with TRAIL stimulation alone in G361 (Fig. 6). In IFN-sensitive melanoma cell lines, IFN-β pretreatment followed by TRAIL stimulation reduced the cell viability of SK-mel-23 compared with IFN-β treatment alone, although exogenous apoptosis-inducing ligands treatment did not reduce its cell viability. However, IFN-β pretreatment followed by any apoptosis-inducing ligands did not reduce the cell viability of MM418 compared with IFN-β treatment alone. In IFN-resistance G361 cells, IFN-β pretreatment followed by TRAIL stimulation significantly reduced cell viability compared with that of TRAIL treatment alone.

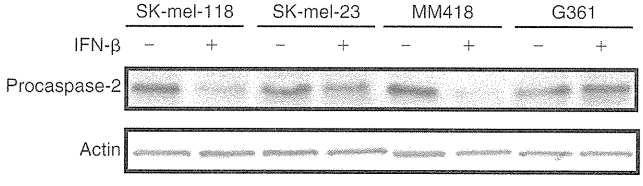


FIG. 4. Activation of caspase-2 detected with degradation of procaspase-2 protein by Western blotting. The cells were treated with interferon (IFN)-β at 1,000 IU/mL for 48 h. The treated cells were lysed, and processed to Western blotting.

IFN-β pretreatment enhanced up-regulation of caspase-2 activity in G361 treated with TRAIL.

We next analyzed the up-regulation of caspase activity of G361, which is an IFN-resistant cell line, when cells were treated with TRAIL, and with IFN-β followed by TRAIL. The cells treated with TRAIL showed up-regulation of caspase-2 and -3 activities as did IFN-sensitive cell lines, in which IFN-β induced apoptosis. Furthermore, IFN-β pretreatment

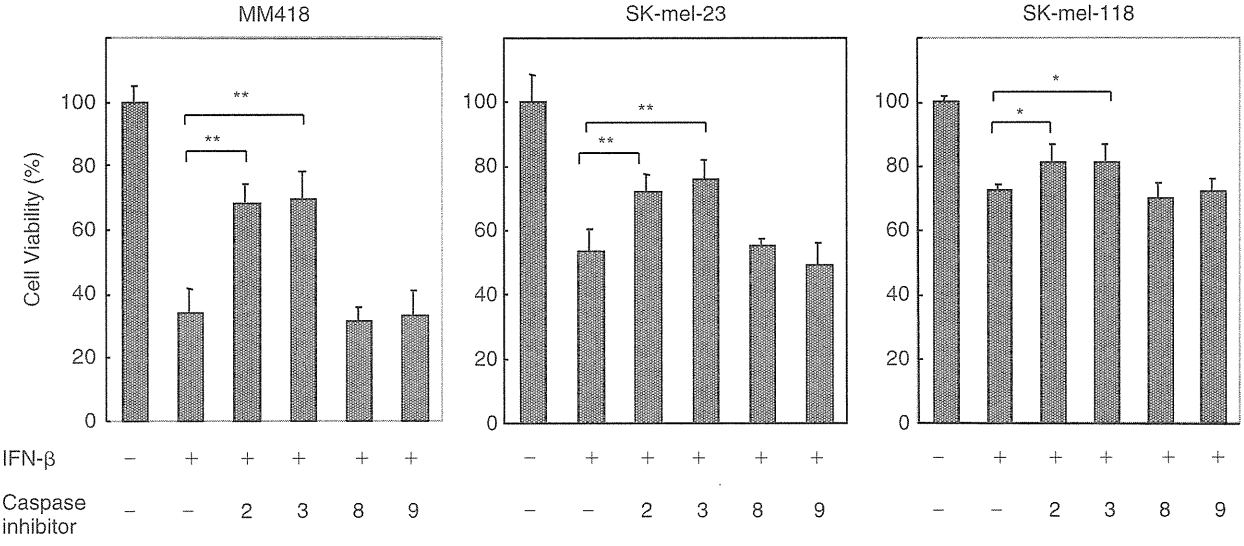


FIG. 5. Effect of caspase inhibitors on interferon (IFN)-β-induced apoptosis. The cells were treated with IFN-β at 1,000 IU/mL in the presence of caspase inhibitor (specific for caspase-2, -3, -8, or -9) at a concentration of 100 mM. After 48 h treatment, cell viability was determined by MTT assay. Each experiment was performed in quadraplicate. The results are expressed as relative values (mean ± S.D.) to untreated controls. $^{**}P < 0.01$, $^{*}P < 0.05$.

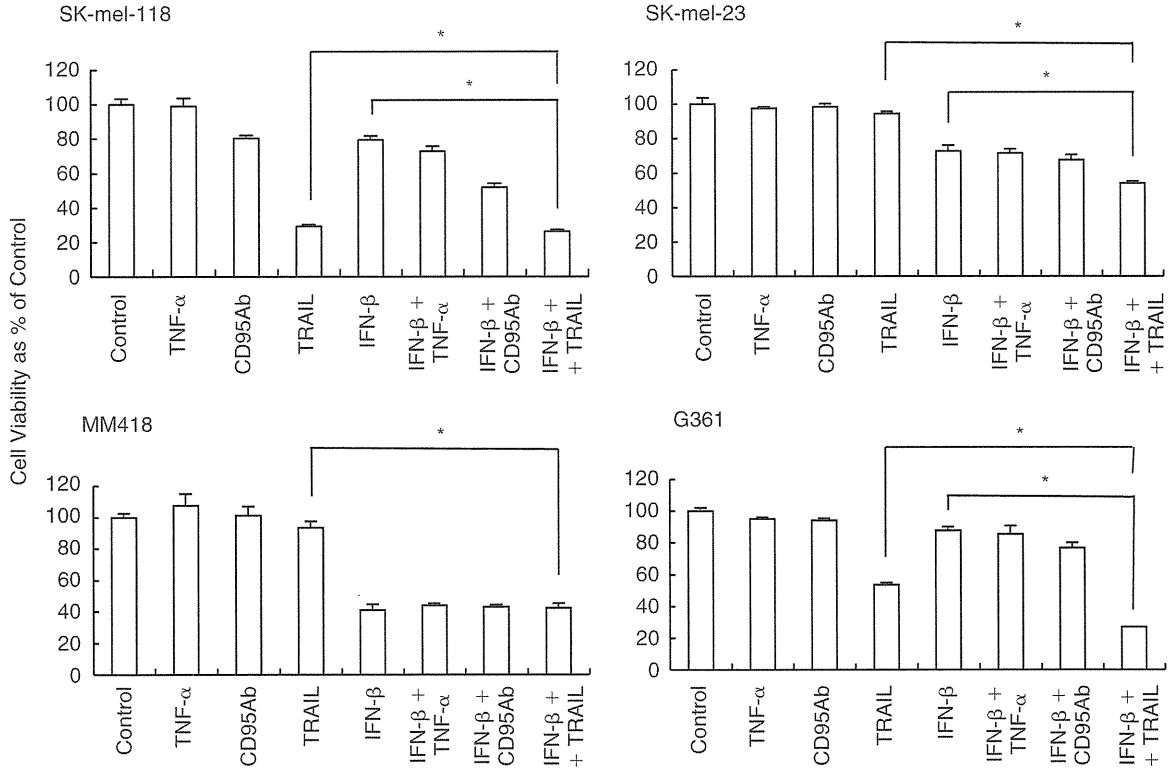


FIG. 6. Cell viability assay after treatment with exogenous apoptosis-inducing ligands and interferon (IFN)-β pretreatment followed by apoptosis-inducing ligands. Cells were plated in 96-well plates with $1 \times 10^3$ cells/well. Cells were treated with TNF-α, the anti-Fas (CD95) antibody, or tumor necrosis factor-related apoptosis-inducing ligand (TRAIL) for 48 h at the concentrations of 50, 500, and 100 ng/mL, respectively, or with 1,000 IU/mL IFN-β (24 h) pretreatment followed by apoptosis-inducing ligands for 48 h at the same concentrations as above. Cell viability was determined by the formazan-formation assay in triplicate. The results are expressed as relative values (mean ± S.D.) to untreated controls.

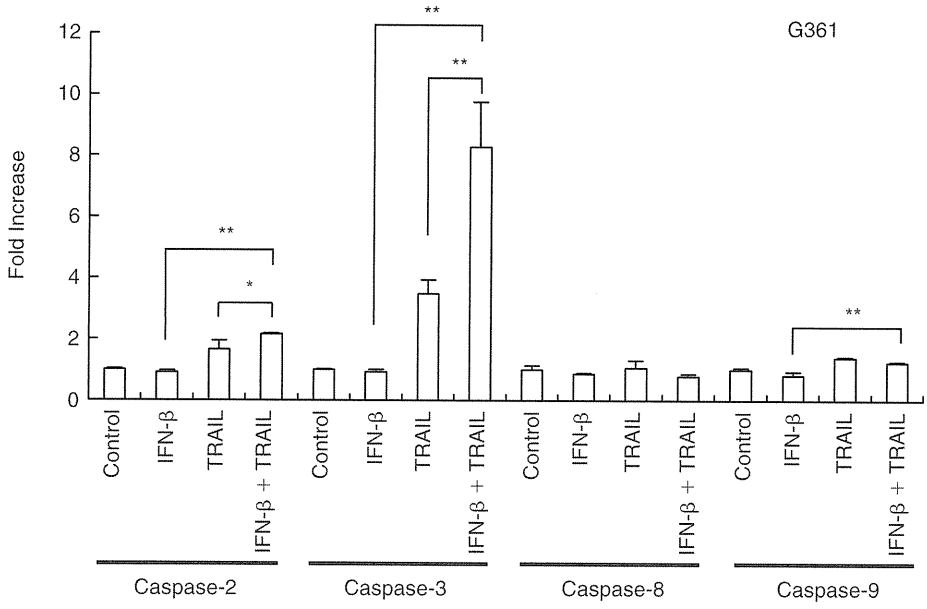


FIG. 7. Caspase assay after treatment with apoptosis-inducing ligands and interferon (IFN)-β pretreatment followed by apoptosis-inducing ligands. G361 cells were plated in a 10-cm dishes with $2 \times 10^4$ cells/mL. Cells were treated with TRAIL for 24 h at the concentration of 100 ng/mL, or with 1,000 IU/mL IFN-β (24 h) pretreatment followed by a PBS wash and addition of TRAIL for 24 h at the same concentration as above. Cells were harvested and caspase activity was assessed by caspase fluorometric assay as in the manufacturer's protocol. The caspase activity is expressed as the fold increase compared with the untreated cells. TRAIL, tumor necrosis factor-related apoptosis-inducing ligand; TNF-α, tumor necrosis factor α; *significant ($P$ <0.01) difference.

enhanced the up-regulation of caspase-2 and -3 (Fig. 7), correlated with inducibility of apoptosis (Fig. 6).

## Discussion

In this study we found that cell death was promoted by IFN-α2 and -β treatments in human melanoma cell lines (SK-mel-118, SK-mel-23, and MM418), and that IFN-β preferentially induced cytotoxic effects compared to IFN-α2. We also found that this cell death induced by IFN-β was induced by apoptosis.

It has been reported that IFN-β treatment induces apoptosis that is dependent on TRAIL induction in melanoma cells. It was indicated that the cells that failed to express TRAIL after IFN-β treatment were resistant to IFN-induced apoptosis, whereas those that induced TRAIL by IFN-β were sensitive to IFN-induced apoptosis (Chawla-Sarkar and others 2001). The induction of TRAIL by IFN-β has been shown to initiate the apoptotic cascade in a wide variety of tumor cells (Shin and others 2005; Vogler and others 2007). It was shown in melanoma cells that TRAIL had a more significant tumoricidal effect than other members of the tumor necrosis factor family such as TNF-α and Fas ligand (Griffith and others 1998). We also showed a similar result that TRAIL had more significant apoptotic effect than the other apoptosis-inducing ligands, such as TNF-α and anti-Fas antibody, in TRAIL-sensitive cell lines, SK-mel-118 and G361 (Fig. 6). The induction of TRAIL by IFN-β was shown to be necessary, but still insufficient to induce apoptosis (Chawla-Sarkar and others 2002). In our study 2 melanoma cell lines, SK-mel-118 and SK-mel-23, exhibited such biological reactions in IFN-β-induced apoptosis, and markedly up-regulated TRAIL mRNA in response to IFN-β treatment. In contrast, in G361, in which ISGs were induced by IFN-β treatment, IFN-β did not induce apoptosis and significant expression of TRAIL mRNA, although exogenous TRAIL induced apoptotic cell death. However, anti-TRAIL antibody slightly suppressed IFN-β-induced apoptosis but did not show any significant anti-apoptotic effect by IFN-β on SK-mel-118 and SK-mel-23 cells. These results indicated that a TRAIL-independent pathway may exist, although TRAIL expression contributes to IFN-β-induced apoptosis to some extent.

Our study showed a new and unique finding in the study of MM418. MM418 significantly underwent apoptosis induced by IFN-β treatment but did not exhibit significant expression of TRAIL mRNA (Fig. 1B). Furthermore, exogenous TRAIL did not induce apoptosis in MM418, and caspase-2 activation of MM418 by IFN-β treatment was much higher than in SK-mel-118 and SK-mel-23, which are thought to undergo TRAIL-mediated apoptosis to some extent. These findings suggested that MM418 cells underwent apoptosis via an alternative pathway, such as a TRAIL-independent apoptotic pathway induced by IFN-β.

Several recent studies demonstrated TRAIL-mediated apoptosis through the caspase-2 pathway in other tumor cell lines (Wagner and others 2004; Shin and others 2005). They suggested that caspase-2 was required in the upstream of Bid, which leads to caspase-9 activation in the mitochondrial apoptotic pathway (Wagner and others 2004; Bonzon and others 2006). Samraj and others indicated that caspase-2 activation was absent in a mutant Jurkat T-cell line with a defect of caspase-9 when treated with an anticancer drug releasing cytochrome *c* (Samraj and others 2007). Shin and others

also indicated that caspase-2 processed procaspase-8 (Shin and others 2005). Thus caspase-2 appears to have diverse functions in apoptotic processes. Our study suggested the possible presence of an alternative IFN-induced apoptotic pathway that activates caspase-2 directly without induction of TRAIL. In a previous study, TRAIL was indicated to be a novel therapeutic modality useful for the management of melanomas (Ren and others 2004). We, however, identified TRAIL-independent IFN-β-induced apoptosis in one cell line, MM418.

Another new finding in this study was for G361. It did not show IFN-β-mediated apoptosis, but its IFN signal transduction seemed to be normal. Griffith and others previously reported that only TRAIL among apoptosis-inducing ligands had a significant cytotoxic effect (Griffith and others 1998). In this study TRAIL mRNA was not induced by IFN-β in G361, although other ISGs were expressed. Thus, this loss of TRAIL-mRNA induction may be a meaningful biological process for the resistance to IFN-β-induced apoptosis because exogenous TRAIL induced significant apoptosis in G361 (Fig. 6). It has also been suggested that IFN-β pretreatment sensitizes TRAIL-mediated apoptosis (Chawla-Sarkar and others 2002). In this study, we also showed that IFN-β pretreatment increased sensitivity against TRAIL-mediated apoptosis in G361 and SK-mel-23, SK-mel-118. When G361 was treated with IFN-β followed by additional TRAIL treatment, caspase-2 activity was up-regulated compared with that after TRAIL treatment alone. Thus not only TRAIL but also other factors induced by IFN seem to be important for apoptotic processes, because synergetic activity of TRAIL and IFN-β treatment was observed in this study after treatment with TRAIL and IFN-β in G361 and specifically in SK-mel-23, in which TRAIL alone did not induce apoptosis although IFN-β pretreatment enhanced apoptosis by TRAIL stimulation. Along with a previous report (Chawla-Sarkar and others 2002), we found in this study that the TRAIL/caspase-2 system was important for induction of apoptosis in 3 (SK-mel-118, SK-mel-23, G361) of the 4 melanoma cell lines tested. On the other hand, in MM418 IFN-induced caspase-2 and -3 activation and apoptosis occurred without TRAIL expression.

Our results further suggested that those melanoma cell lines (SK-mel-118, SK-mel-23, MM418), in which apoptosis was induced by IFN-β, commonly had up-regulated caspase-2 activity with (SK-mel-118, SK-mel-23) or without (MM418) involvement of a TRAIL-related pathway. Furthermore, caspase-2 and -3 inhibitors remarkably suppressed IFN-β-induced apoptosis that was equivalent to that in IFN-β-sensitive cell lines. The finding was a common phenomenon in these cell lines, and the increased apoptotic population had up-regulation on caspase-2 activity, but not on TRAIL induction.

Thus our present results clearly indicate that the extent of the IFN-β-induced apoptosis depends on up-regulation of caspase-2 activity more strongly than on induction of TRAIL. These findings suggest that measurement of caspase-2 activity in primary culture cells from excised melanoma tissues can be a novel marker for estimating the extent of the cytotoxic effect of IFN-β adjuvant therapy for melanoma. Caspase-2 activity may be useful for IFN-induced sensitization of chemotherapeutic drugs to melanoma cells.

## Acknowledgments

We are indebted to Drs. Akinori Kawakami, Kenji Yanagisawa and Masae Okura of Sapporo Medical University for their valuable contributions. This study was supported by Grants-in Aid for Scientific Research from the Ministry of Education, Culture, Sports, Science and Culture, Japan (16390319, 16024218) and the Ministry of Health, Labour and Welfare, Japan (H17-nano-004).

## Author Disclosure Statement

No competing financial interests exist.

## References

Bonzon C, Bouchier-Hayes L, Pagliari LJ, Green DR, Newmeyer DD. 2006. Caspase-2-induced apoptosis requires bid cleavage: a physiological role for bid in heat shock-induced death. Mol Biol Cell 17(5):2150–2157.

Chawla-Sarkar M, Leaman DW, Borden EC. 2001. Preferential induction of apoptosis by interferon (IFN)-beta compared with IFN-alpha2: correlation with TRAIL/Apo2L inductioni nm elanomac elll ines. ClinC ancerR es 7(6):1821–1831.

Chawla-Sarkar M, Leaman DW, Jacobs BS, Borden EC. 2002. IFN-beta pretreatment sensitizes human melanoma cells to TRAIL/Apo2l igand-induceda poptosis. JI mmunol 169(2):847–855.

Chawla-Sarkar M, Lindner DJ, Liu YF, Williams BR, Sen GC, Silverman RH, Borden EC. 2003. Apoptosis and interferons: role of interferon-stimulated genes as mediators of apoptosis. Apoptosis 8(3):237–249.

Chen Q, Gong B, Mahmoud-Ahmed AS, Zhou A, Hsi ED, Hussein M, Almasan A. 2001. Apo2L/TRAIL and Bcl-2-related proteins regulate type I interferon-induced apoptosis in multiple myeloma. Blood 98(7):2183–2192.

Fisher PB, Prignoli DR, Hermo H, Jr., Weinstein IB, Pestka S. 1985. Effects of combined treatment with interferon and mezerein on melanogenesis and growth in human melanoma cells. J Interferon Res 5(1):11–22.

Griffith TS, Chin WA, Jackson GC, Lynch DH, Kubin MZ. 1998. Intracellular regulation of TRAIL-induced apoptosis in human melanomac ells. JI mmunol 161(6):2833–2840.

Kang DC, Gopalkrishnan RV, Lin L, Randolph A, Valerie K, Pestka S, Fisher PB. 2004. Expression analysis and genomic characterization of human melanoma differentiation associated gene-5, mda-5: a novel type I interferon-responsive apoptosis-inducing gene. Oncogene 23(9):1789–1800.

Kimberley FC, Screaton GR. 2004. Following a TRAIL: update on a ligand and its fiver eceptors. CellR es 14(5):359–372.

Leaman DW, Chawla-Sarkar M, Jacobs B, Vyas K, Sun Y, Ozdemir A, Yi T, Williams BR, Borden EC. 2003. Novel growth and death related interferon-stimulated genes (ISGs) in melanoma: greater potency of IFN-beta compared with IFN-alpha2. J Interferon CytokineR es 23(12):745–756.

Meng RD, El-Deiry WS. 2001. p53-independent upregulation of KILLER/DR5 TRAIL receptor expression by glucocorticoids and interferon-gamma. ExpCe llR es 262(2):154–169.

Merchant MS, Yang X, Melchionda F, Romero M, Klein R, Thiele CJ, Tsokos M, Kontny HU, Mackall CL. 2004. Interferon gamma enhances the effectiveness of tumor necrosis factor-related apoptosis-inducing ligand receptor agonists in a xenograft model of Ewing's sarcoma. Cancer Res 64(22):8349–8356.

Morrison BH, Tang Z, Jacobs BS, Bauer JA, Lindner DJ. 2005. Apo2L/TRAIL induction and nuclear translocation of inositol hexakisphosphate kinase 2 during IFN-beta-induced apoptosis ino varianc arcinoma. BiochemJ 385(Pt2 ):595–603.

Pfeffer LM, Dinarello CA, Herberman RB, Williams BR, Borden EC, Bordens R, Walter MR, Nagabhushan TL, Trotta PP, Pestka S. 1998. Biological properties of recombinant alpha-interferons: 40th anniversary of the discovery of interferons. Cancer Res 58(12):2489–2499.

Ren DH, Mayhew E, Hay C, Li H, Alizadeh H, Niederkorn JY. 2004. Uveal melanoma expression of tumor necrosis factor-related apoptosis-inducing ligand (TRAIL) receptors and susceptibility to TRAIL-induced apoptosis. Invest Ophthalmol Vis Sci 45(4):1162–1168.

Reu FJ, Leaman DW, Maitra RR, Bae SI, Cherkassky L, Fox MW, Rempinski DR, Beaulieu N, MacLeod AR, Borden EC. 2006. Expression of RASSF1A, an epigenetically silenced tumor suppressor, overcomes resistance to apoptosis induction by interferons. Cancer Res 66(5):2785–2793.

Samraj AK, Sohn D, Schulze-Osthoff K, Schmitz I. 2007. Loss of caspase-9 reveals its essential role for caspase-2 activation and mitochondrialm embraned epolarization. MolB iolCe ll 18(1):84–93.

Shin S, Lee Y, Kim W, Ko H, Choi H, Kim K. 2005. Caspase-2 primes cancer cells for TRAIL-mediated apoptosis by processing procaspase-8. EMBOJ 24(20):3532–3542.

Stark GR, Kerr IM, Williams BR, Silverman RH, Schreiber RD. 1998. How cells respond to interferons. Annu Rev Biochem 67:227–264.

van Loo G, Saelens X, Matthijssens F, Schotte P, Beyaert R, Declercq W, Vandenabeele P. 2002. Caspases are not localized in mitochondria during life or death. Cell Death Differ 9(11):1207–1211.

Vogler M, Dürr K, Jovanovic M, Debatin KM, Fulda S. 2007. Regulation of TRAIL-induced apoptosis by XIAP in pancreatic carcinomac ells. Oncogene 26(2):248–257.

Wagner KW, Engels IH, Deveraux QL. 2004. Caspase-2 can function upstream of bid cleavage in the TRAIL apoptosis pathway. J Biol Chem 279(33):35047–35052.

Yamashita T, Tokino T, Tonoki H, Moriuchi T, Jin HY, Omori F, Jimbow K. 2001. Induction of apoptosis in melanoma cell lines byp 53a ndi tsr elatedp roteins. JI nvestD ermatol 117(4):914–919.

Zhang L, Fang B. 2005. Mechanisms of resistance to TRAIL-induced apoptosisi nc ancer. CancerG eneT her 12(3):228–237.

Zhivotovsky B, Orrenius S. 2005. Caspase-2 function in response to DNAd amage. BiochemB iophysR esC ommun 331(3):859–867.

Zhivotovsky B, Samali A, Gahm A, Orrenius S. 1999. Caspases: their intracellular localization and translocation during apoptosis. CellD eathD iffer 6(7):644–651.

Address correspondence to:
*Dr. Kowichi Jimbow*
*Institute of Dermatology & Cutaneous Sciences 1-27*
*Odori W-17*
*Chuoku, Sapporo 0600042*
*Japan*

*E-mail:* jimbow@sapmed.ac.jp

Received 6 February 2009/Accepted 21 September 2009

Biochimica et Biophysica Acta 1800 (2010) 669–673

Contents lists available at ScienceDirect

Biochimica et Biophysica Acta

journal homepage: www.elsevier.com/locate/bbagen

# Agaritine purified from *Agaricus blazei* Murrill exerts anti-tumor activity against leukemic cells

Masahiro Endo [a,g,1], Hidehiko Beppu [b,*], Hidehiko Akiyama [c], Kazumasa Wakamatsu [d], Shosuke Ito [d], Yasuko Kawamoto [e], Kan Shimpo [b], Toshimitu Sumiya [f], Takaaki Koike [g], Taei Matsui [a]

[a] *Department of Biology, Faculty of Medical Technology, Fujita Health University School of Health Sciences, Toyoake, Aichi 470-1192, Japan*
[b] *Fujita Memorial Nanakuri Institute, Fujita Health University, Tsu, Mie 514-1296, Japan*
[c] *Department of Clinical Hematology, Faculty of Medical Technology, Fujita Health University of Health Sciences, Toyoake, Aichi 470-1192, Japan*
[d] *Department of Chemistry, Faculty of Medical Technology, Fujita Health University School of Health Sciences, Toyoake, Aichi 470-1192, Japan*
[e] *Department of Microbiology, Faculty of Medical Technology, Fujita Health University School of Health Sciences, Toyoake, Aichi 470-1192, Japan*
[f] *Iwade Research Institute of Mycology, Tsu, Mie 514-0012, Japan*
[g] *Department of Clinical Laboratory Sciences, Faculty of Medical Technology, Fujita Health University School of Health Sciences, Toyoake, Aichi 470-1192, Japan*

ARTICLE INFO

*Article history:*
Received 13 January 2010
Received in revised form 16 March 2010
Accepted 19 March 2010
Available online 27 March 2010

*Keywords:*
*Agaricus blazei*
Agaritine
Anti-tumor activity
Leukemic cell
Non-carcinogenicity

ABSTRACT

*Background:* Mushrooms of the genus *Agaricus* are a common folk remedy against carcinoma. The active ingredients, polysaccharides and protein-polysaccharide complexes containing β-glucan, have been isolated and shown to have indirect tumor-suppressing activity via an immunological activation.
*Methods:* The diffusible fraction of a hot-water extract of *Agaricus blazei* Murrill (ABM) powder was fractionated by HPLC based on the anti-tumor activity against leukemic cells *in vitro*. The structure of the anti-tumor substance was determined by NMR and MS analyses.
*Results:* We purified a tumorcidal substance from the diffusible fraction of ABM and identified it as agaritine, β-*N*-(γ-L(+)-glutamyl)-4-(hydroxymethyl) phenylhydrazine, having a molecular mass of 267 Da. This compound inhibited the proliferation of leukemic cell lines such as U937, MOLT4, HL60 and K562 with $IC_{50}$ values of 2.7, 9.4, 13.0, and 16.0 μg/mL, respectively, but showed no significant effect on normal lymphatic cells at concentrations up to 40 μg/mL. Although agaritine has been suspected of having genotoxic or carcinogenic properties, agaritine did not activate the *umu* gene of *Salmonella*, which reacts to carcinogens.
*General significance:* The results indicate that agaritine from ABM has direct anti-tumor activity against leukemic tumor cells *in vitro*. This is in contrast to the carcinogenic activity previously ascribed to this compound. Our results also show that this activity is distinct from that of β-glucan, which indirectly suppresses proliferation of tumor cells.



## 1. Introduction

Mushrooms of the genus *Agaricus* contain, in addition to several minerals, vitamins and dietary fibers, bioactive substances such as immunopotentiating substances which are believed to suppress cancer progression or metastasis [1]. In particular, β-glucan (β1-3, β1-6 linked glucan) from these mushrooms has been reported to act as an immuno-accelerator against cancer cells [2,3]. β-glucans such as lentinan from *Lentinula edodes* [4], schizophyllan from *Schizophyllum commune* [5], and the polysaccharide kureha (krestin) from *Coriolus versicolor* [6] are known to be biological response modifiers for macrophages, T cells and NK cells. These compounds induce the activation of the immune response, and have been clinically used as anti-cancer drugs in combination with other drugs [7–9].

*Agaricus blazei* Murrill (ABM) is a commonly used folk remedy against carcinoma. The polysaccharides and protein-polysaccharide complexes containing β-glucan have been isolated [1,10,11]. In the present study, we found that the heat-stable and diffusible fraction of ABM has anti-tumor activity *in vitro*. This substance directly decreased the viability of leukemic cell lines but had no effect on normal lymphocytes. Structural analysis revealed that the anti-tumor substance is agaritine, a hydrazine-containing compound. Although a carcinogenic effect of ABM has been reported, and agaritine or metabolic derivatives of agaritine are suspected to be genotoxic,

*Abbreviations:* ABM, *Agaricus blazei* Murrill; FCS, fetal calf serum; HPLC, high-performance liquid chromatography; MQ water, milli Q water; MS, mass spectrometry; NMR, nuclear magnetic resonance

* Corresponding author. Fujita Memorial Nanakuri Institute, Fujita Health University, 1865 Hisai-isshiki-sho, Tsu, Mie 514-1296, Japan. Tel.: +81 59 252 1010; fax: +81 59 252 0710.
*E-mail addresses:* hbeppu@fujita-hu.ac.jp (H. Beppu), hakiyama@fujita-hu.ac.jp (H. Akiyama), kwaka@fujita-hu.ac.jp (K. Wakamatsu), sito@fujita-hu.ac.jp (S. Ito), ykawamot@fujita-hu.ac.jp (Y. Kawamoto), shimpo@fujita-hu.ac.jp (K. Shimpo), estrella@iwade101.com (T. Sumiya), tmatsui@fujita-hu.ac.jp (T. Matsui).
[1] Present address: Daiichi-Sankyo RD Associe Co. Ltd., Shinagawa, Tokyo, 140-0001, Japan.

0304-4165/$ – see front matter © 2010 Elsevier B.V. All rights reserved.
doi:10.1016/j.bbagen.2010.03.016

carcinogenic or tumorigenic agents [12–15], the present study shows that, according to the *umu* test, agaritine has no carcinogenic effect. This is the first report that clearly indicates the anti-tumor effects of agaritine *in vitro*.

## 2. Materials and methods

### 2.1. Materials

Lyophilized ABM powder was obtained from Nanakuri Institute, Fujita Health University (bulk powder from Iwade Research Institute of Mycology, Tsu, Mie, Japan). Milli Q (MQ) water (Millipore, Tokyo, Japan) was used throughout the experiments. Dialysis membrane, which excludes molecules less than 10 kDa in mass, was purchased from Spectrum Laboratories (Rancho Dominguez, CA, USA). Synthetic agaritine, procarbazine-HCl and other chemicals of the highest purity available were purchased from Wako Pure Chemicals (Osaka, Japan).

### 2.2. Cells

U937, MOLT4, HL60 and K562 cells were obtained from American Type Culture Collection or Aichi Cancer Research Center (Nagoya, Japan). Cells were cultured in RPMI-1640 medium (Sigma-Aldrich, Tokyo, Japan) supplemented with 10% heat-inactivated fetal calf serum (FCS), 100 units/mL penicillin and 100 μg/mL streptomycin. Cells were placed into 50-$cm^2$ tissue culture flasks and grown at 37 °C under an atmosphere of 5% $CO_2$ in air. Peripheral blood mononuclear cells (normal lymphocytes) collected from healthy donors (after receipt of informed consent) were separated by density gradient centrifugation using Isoprep (Robbins Scientific, Sunnyvale, CA, USA) or Histopaque-1077 (Sigma-Aldrich) and cultured in RPMI-1640 medium as above.

### 2.3. Extraction of the anti-tumor substance

ABM powder (20 g) was boiled in MQ water (2000 mL) for 2 h, and the hot-water extract was chilled, filtrated through Advantech No.2 filter paper (Osaka, Japan) and evaporated to dryness (13.9 g). The dried filtrate was dissolved in MQ water (0.4 g/mL) and dialyzed at 25 °C twice against 750 volumes of MQ water for 2 h, then for 4 h once, using 10 kDa cut off dialysis membrane. The total diffusible fraction was evaporated to dryness and used as the starting material (10.0 g). The remaining solution in the bag (non-diffusible fraction) was also evaporated to dryness (2.1 g).

### 2.4. Fractionation of the anti-tumor substance by high-performance liquid chromatography (HPLC)

Dry powder of diffusible fraction was dissolved in MQ water (333 mg/mL) and centrifuged at 12,000 rpm for 10 min at 25 °C. The supernatant was passed through a cartridge filter (Millex LCR, 0.2 μm, Millipore) and aliquots (30 mg) were subjected to HPLC on an YMC-Pack ODS AQ column (10 mm × 250 mm, YMC, Kyoto, Japan) equilibrated with MQ water. The column was washed and eluted with a linear gradient of methanol into aqueous MQ water. The eluent was monitored by absorbance (ABS) at 280 nm, and fractions were collected and concentrated by evaporation (after identification of agaritine, a wavelength of 238 nm was used, as this compound shows maximum absorbance at this wavelength). Fractions with anti-tumor activity were subjected to second round of chromatography on an YMC-Pack ODS AQ column (4.7 mm × 250 mm, YMC) equilibrated and eluted with MQ water.

### 2.5. Structural analysis of the anti-tumor substance

The elucidation of structure of purified substance (3.9 mg) with anti-tumor activity was performed by mass spectrometry (MS), $^1$H-nuclear magnetic resonance (NMR) and $^{13}$C-NMR spectra. Mass analysis was performed by the liquid chromatography/mass spectrometry/mass spectrometry (LC/MS/MS) analysis using an electrospray ionization/ion trap mass spectrometer, an ESI-API 3000 (Applied Biosystems, Carlsbad, CA, USA), and a JMS-700QQ FAB-MS (JEOL, Tokyo, Japan), and NMR was performed at Takara Bio (Ohtsu, Japan) using an Avance 600 (Bruker Biospin, Yokohama, Japan). The MS analysis was carried out directly by the MS/MS at positive ion mode; $[M+H]^+$: $m/z$ 268, 250, 232, 186. $^1$H-NMR was measured at 600 MHz ($D_2O$): 2.00 ppm (2H, s), 2.33 ppm (2H, m), 3.60 ppm (1H, s), 4.34 ppm (2H, s), 6.69 ppm (2H, m), 7.09 ppm (2H, m). $^{13}$C-NMR was measured at 150 MHz ($D_2O$): 26.4 ppm ($CH_2$), 29.8 ppm ($CH_2$), 54.4 ppm (CH), 63.9 ppm ($CH_2OH$), 113.7 ppm (CH, aromatic carbon), 129.4 ppm (CH, aromatic carbon), 133.0 ppm (C, aromatic carbon), 147.1 ppm (C, aromatic carbon), 174.2 ppm (COOH), 175.1 ppm (CO). The structure was furthermore clarified by using 2D-NMR and $^{13}$C-NMR-DEPT (Distorsionless Enhancement by Polarization Transfer) 135 methods (data not shown).

### 2.6. Assay for anti-tumor activity

U937, MOLT4, HL60, K562 and normal lymphocyte cells were grown in RPMI-1640 medium containing 10% FCS at 37 °C and 5% $CO_2$. Cell suspensions (90 μL, $4 \times 10^5$/mL) were then incubated with each test solution (10 μL) in a 96-well plate for up to 48 h. Cell survival/proliferation was measured by a Cell Counting Kit-8 (Dojindo, Tokyo, Japan) using water-soluble disulfonated tetrazolium salt (WAT-8) [16]. Briefly, 10 μL of WAT-8 solution was added to each well and the absorbance at 492/620 nm was measured with a Multiskan Bichromatic microplate reader (LabSystems, Bucharest, Romania) after 2 h. Survival rates of the cells were determined and the $IC_{50}$ values were calculated.

### 2.7. Carcinogenicity test

Carcinogenicity was monitored by the *umu* test using an Umulac AT kit (Jimuro Co. Ltd, Takasaki, Japan) according to the instruction manual [17]. This method is based on the expression of the *umu* gene, which is activated by mutagens. Briefly, a suspension of *Salmonella typhimurium* (NM2009 strain) possessing the *umu* gene conjugated with the β-galactosidase gene was mixed with agaritine (final concentration 1–8 μg/mL) in the presence or absence of cofactor (S9, rat liver homogenate) and incubated for 2 h at 37 °C. Substrate solution (X-gal) was added and absorbance at 620 nm was measured after 1 h. 2-(2-furyl)-3-(5-nitro-2-furyl) acrylamide (2-AF, 0–0.3 μg/mL, without S9) and 2-aminoanthracene (2-AA, 0–0.3 μg/mL, with S9) were used as positive carcinogens.

## 3. Results

### 3.1. Purification of the anti-tumor substance

The hot-water extract of ABM suppressed the viability of U937 cells by approximately 40% (Fig. 1). To eliminate high-molecular-weight β-glucan, the hot-water extract was extensively dialyzed against water to separate diffusible small molecules from non-diffusible large molecules. Although the non-diffusible fraction in the dialysis bag showed weak activity at higher concentration, the anti-tumor activity was mainly recovered from the diffusible fraction, indicating that the major anti-tumor substance is a heat-stable small molecule(s) such as a carbohydrate, peptide or other organic compound(s). The diffusible fraction was fractionated by HPLC into five fractions (I–V, Fig. 2A). Since fraction II showed comparatively stronger activity (Fig. 2B), it was repeatedly chromatographed on the HPLC column until a single peak was obtained (Fig. 3A). Finally, 4.1 mg of anti-tumor substance was purified from 20 g of ABM powder. The purified anti-tumor substance showed high tumor-suppression activity, with an $IC_{50}$ value of 6.1 μg/

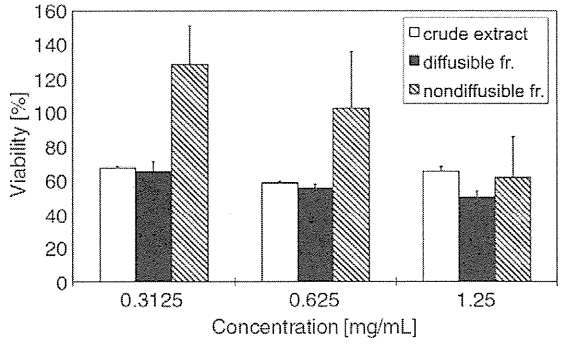


**Fig. 1.** Effects of ABM extract and dialyzed extract on the viability of U937 cells. Hot-water extract of ABM and diffusible/non-diffusible fractions obtained by extensive dialysis of the hot-water extract were added to U937 cells at concentrations ranging from 0.31 to 1.25 mg/mL. After 48 h, cell viability was assayed using a Cell Counting Kit-8. Anti-tumor activity found in the hot-water extract was largely recovered in the diffusible fraction after dialysis.

mL (Fig. 3B). Since the crude diffusible fraction showed 50% inhibition of U937 proliferation at 1.25 mg/mL (Fig. 1), an approximately 200-fold purification was achieved by the HPLC procedure.

### 3.2. Structure of the anti-tumor substance

The purified anti-tumor substance was white in color, highly soluble in water, methanol, and ethanol, and showed maximum absorbance at 238 nm. LC/MS analysis showed that it has a molecular mass of 267 Da

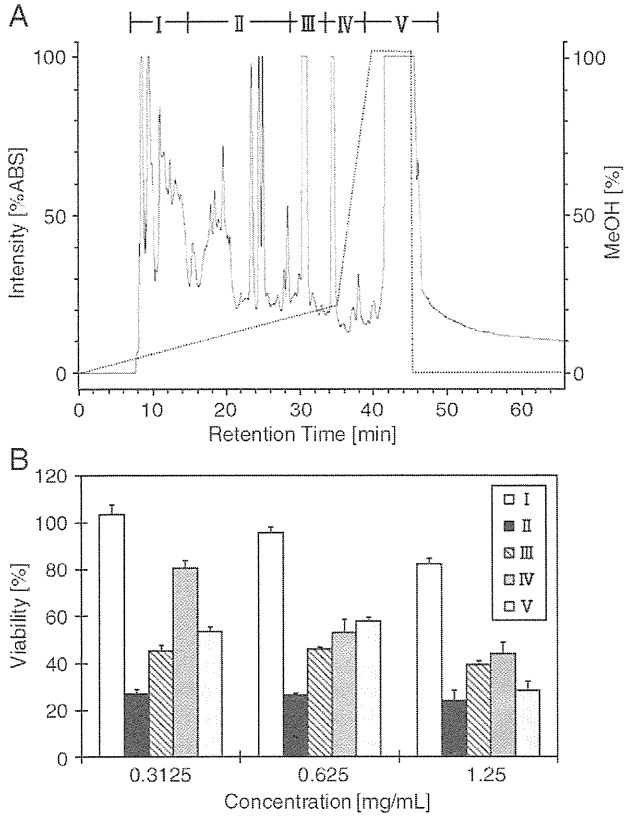


**Fig. 2.** Fractionation of anti-tumor substances from ABM by HPLC. (A) The diffusible fraction was fractionated into five fractions (I to V) by HPLC on an YMC-Pack ODS AQ column (10 mm × 250 mm) using a methanol gradient (dotted line). (B) Each fraction was assayed for cell viability using U-937 cells. Several fractions exhibited anti-tumor activity, with fraction II showing the highest activity.

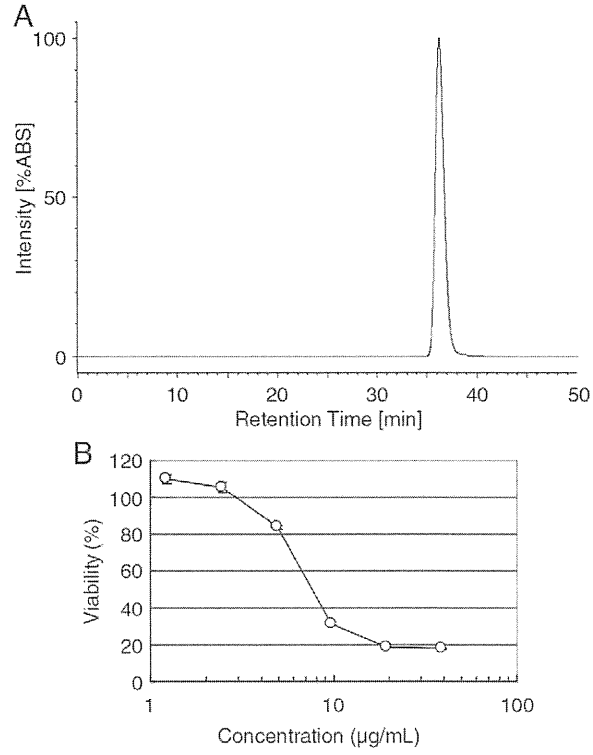


**Fig. 3.** Purification of the anti-tumor substance. (A): Fraction II in Fig. 2A was repeatedly subjected to HPLC on the same column to provide a single peak fraction. (B) The peak fraction in panel A showed strong suppressive activity towards U937 cells, with an $IC_{50}$ value of 6.1 μg/mL.

(data not shown). $^{13}$C-NMR and $^{1}$H-NMR analysis, together with the MS data, suggested that the anti-tumor substance is identical to agaritine, β-*N*-(γ-L(+)-glutamyl)-4-(hydroxymethyl) phenylhydrazine ($C_{12}H_{17}O_4N_3$, 267 Da), previously purified from *A. bisporus* [18] and a compound synthesized by Wallcave et al. [19] (Fig. 4). Commercially available synthetic agaritine showed the same retention time and absorbance spectrum as that of the purified anti-tumor substance (data not shown).

### 3.3. Effects of agaritine on the viability of leukemic cells and normal lymphocytes

Synthetic agaritine was assayed to determine whether it shows anti-tumor activity *in vitro*. As shown in Fig. 5, agaritine suppressed U937 with an $IC_{50}$ value of 2.7 μg/mL, which is comparable to that of the purified anti-tumor substance from ABM. The higher activity of synthetic agaritine suggests that our preparation still contains some

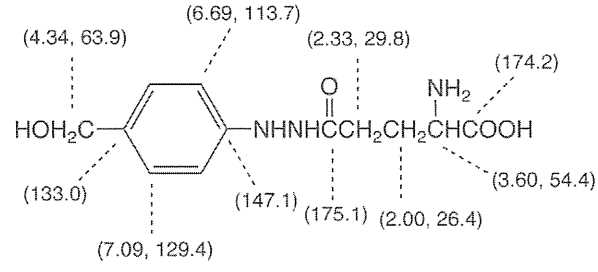


**Fig. 4.** Structure of the anti-tumor substance isolated from ABM. NMR data of the purified anti-tumor substance were expressed as chemical shift values (ppm) of the $^{1}$H-NMR and $^{13}$C-NMR (in parentheses) spectra. The anti-tumor substance purified from ABM was identified as phenylhydrazine containing a glutamyl residue. A hydroxymethyl group is located at the *para* position of the benzene ring.

impurities. Since the anti-tumor substance purified from ABM was identified as agaritine, commercial synthetic agaritine was used in the following experiments.

Other leukemic cell lines (K562, MOLT4 and HL60) and normal lymphocytes were incubated with various concentrations of agaritine for 48 h. The viability of all the leukemic cell lines used decreased as the concentration of agaritine increased (Fig. 5). The $IC_{50}$ values of agaritine to MOLT4, HL60 and K562 were 9.4, 13.0, and 16.0 μg/mL, respectively (Fig. 5). Agaritine had no significant effect on the viability of normal lymphocytes at concentrations up to 40 μg/mL (Fig. 5).

### 3.4. Absence of carcinogenic activity in agaritine

The carcinogenicity of agaritine was examined using the *umu* test (Table 1). Agaritine (1–8 μg/mL) did not activate the *umu* gene of *Salmonella*, which reacts to carcinogens. There was no evidence of carcinogenicity of agaritine even when a cofactor (S9), which metabolically activates promutagens, was added to the *umu* test mixture.

## 4. Discussion

ABM is a commonly used supplemental health food for suppressing cancer, as well as for preventing hypertension, hyperlipemia and diabetes [1]. Polysaccharides of β1-3, β1-6 linked glucose (β-glucan) found in the genus *Agaricus* have been found to suppress cancer by activating immunological responses of macrophages and leukocytes [2,20]. Recently, direct cytotoxic anti-tumor activity of β-glucan has been reported [21–23]. Since ABM also contains β-glucan [1,10,11], its anti-cancer activity might be due to either a direct or indirect effect by β-glucan. The present study showed that an ABM extract not composed of β-glucan directly suppressed proliferation of leukemic cells *in vitro*. This suppressive activity was concentrated in the heat-stable and dialyzable low molecular weight fractions of ABM. The major anti-tumor substance was identified by structural analysis as agaritine, a phenylhydrazine conjugated with glutamic acid. Commercially available synthetic agaritine also showed the same anti-tumor activity. Several other peaks separated by HPLC showed lower-level anti-tumor activity. There is a possibility that these minor active fractions might contain agaritine derivatives. Indeed, fraction IV (Fig. 2A) contained agaritinal, an agaritine derivative containing an aldehyde side chain instead of a hydroxymethyl group, which also showed anti-tumor activity (data not shown).

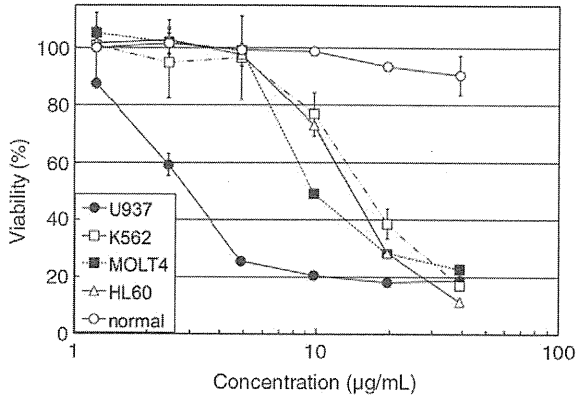


**Fig. 5.** Anti-tumor activity of agaritine against leukemic cells. Leukemic cells (U937, K562, HL60 and MOLT4) and normal lymphocytes were incubated with 0 to 40 μg/mL of agaritine for 48 h. Cell viability was assessed by using Cell Counting Kit-8. Agaritine showed a suppressive effect on all the leukemic cell lines examined, with $IC_{50}$ values of 2.7, 9.4, 13.0, and 16.0 μg/mL for U937, MOLT4, HL60 and K562, respectively, but showed no significant effect on the normal lymphatic cells at concentrations up to 40 μg/mL. Data represent means of three experiments with SD.

**Table 1**
Evaluation of carcinogenicity of agaritine by the *umu* test.

| Without cofactor S9 | | | | With cofactor S9 | | | |
|---|---|---|---|---|---|---|---|
| AF-2 | | Agaritine | | 2-AA | | Agaritine | |
| Conc. | $A_{620}$ | Conc. | $A_{620}$ | Conc. | $A_{620}$ | Conc. | $A_{620}$ |
| 0 | 0.265 | 1.0 | 0.271 | 0 | 0.427 | 1.0 | 0.452 |
| 0.033 | 0.551 | 2.0 | 0.308 | 0.003 | 1.034 | 2.0 | 0.434 |
| 0.1 | 0.749 | 4.0 | 0.255 | 0.03 | 2.239 | 4.0 | 0.432 |
| 0.3 | 1.498 | 8.0 | 0.278 | 0.3 | 1.414 | 8.0 | 0.398 |

Carcinogenicity was monitored by the *umu* test using an Umulac AT kit. A suspension of *S. typhimurium* possessing the *umu* gene conjugated with the β-galactosidase gene was mixed with agaritine (final concentration 1–8 μg/mL) in the presence or absence of cofactor S9 and incubated for 2 h at 37 °C. Substrate solution (X-gal) was added and absorbance at 620 nm was measured after 1 h. AF-2 (2-(2-furyl)-3-(5-nitro-2-furyl) acrylamide, 0–0.3 μg/mL) and 2-AA (2-aminoanthracene, 0–0.3 μg/mL) were used as positive control carcinogens for the *umu* test in the absence or presence of cofactor S9, respectively.

Contrary to its anti-tumor effect, agaritine, either purified or from *Agaricus*, has been suspected of promoting carcinogenicity such as bladder cancer [24]. Several reports of Ames test studies using a *Salmonella* strain suggested that agaritine and its derivatives are potentially mutagenic [12]. Administration of agaritine has been reported to induce cancer or tumors in mice [12], but other reports showed that agaritine had no or an insignificant effect [25,26]. The hydrazine structure has also been considered as a carcinogenic reactant. Such conflicting information regarding the carcinogenicity of agaritine has cast doubt on whether commercial supplements from *Agaricus* mushrooms, or the mushrooms themselves, are safe or toxic, leading to the withdrawal of *Agaricus* supplemental products by some companies. Furthermore, it has been reported that agaritine is unstable in boiling water, or easily degrades in water within 48 h [27]. In contrast, in our purification procedure, agaritine was isolated following boiling and exhaustive dialysis in water, indicating that it is stable towards both heat and water, as reported [18]. One explanation for these discrepancies is that the quality and purity of agaritine previously used for experiments were questionable. In 2008, the Japan National Institute of Health Sciences concluded that agaritine has no significant genotoxicity, based on an *in vivo* study using transgenic mice (Food safety commission working group). Our present results using *Salmonella* species (the *umu* test) also show no carcinogenicity of agaritine in the presence or absence of a metabolic modifier, consistent with the results of Papaparaskeva et al. [28]. Although it is not easy to determine the biological effects of agaritine *in vivo*, current evidence suggests that agaritine and its metabolic derivatives are not carcinogenic. Papaparaskeva et al. (1993) suggested that phenolic and quinonoid compounds may play a significant role in the mutagenicity of mushroom extracts [29].

Possible target for agaritine is not clear at present. Since agaritine is an amphipathic molecule, it can presumably easily penetrate the cell membrane. Our chase-experiments using fluorescein-labeled agaritine and U937 cells showed that agaritine was incorporated into the cytoplasm after binding to the cell surface (unpublished results). The anti-tumor activity might be attributable to the hydrazine structure of agaritine, as several hydrazine compounds have been used as anti-cancer drugs. For example, hydrazine sulfate improves cancerous cachexia, and procarbazine (methylhydrazine) has been used to treat leukemia and non-Hodgkin's malignant lymphoma. However, procarbazine has no effect on the viability of U937 *in vitro* (data not shown). Recently, Gao et al. [30] showed by molecular docking experiments that agaritine and its derivatives have a specific potency to bind HIV proteases. Therefore, agaritines are promising candidates for drug-development in the combat of AIDS.

The mechanism by which agaritine decreases the viability of leukemic cells has not been elucidated. In preliminary experiments, we observed nuclear fragmentation and an increase in annexin V-positive U937 cells after incubation with agaritine. These observations

suggest that agaritine induces apoptosis of leukemic cells. Although agaritine showed no toxic effect on normal lymphocytes, we have not examined the effect of agaritine on cancer cell lines other than leukemic cells. Further studies, including cell and species specificity, effective minimum doses for different cells, and *in vivo* administration using an animal model, are necessary to establish the anti-tumor activity and specificity of agaritine.

## Acknowledgements

The authors are indebted to Dr. N. Hayashi from Tokyo Institute for Technology for the NMR analysis. This work was supported by a research grant from Fujita Health University.

## References

[1] F. Firenzuoli, L. Gori, G. Lombardo, The Medicinal mushroom *Agaricus blazei* Murrill: Review of literature and pharmaco-toxicological problems, Evid-Based Complement. Alternat. Med. 5 (2008) 3–15.
[2] S.P. Wasser, Medicinal mushrooms as a source of antitumor and immunomodulating polysaccharides, Appl. Microbiol. Biotechnol. 60 (2002) 258–274.
[3] D. Akramiene, A. Kondrotas, J. Didziapetriene, E. Kevelaitis, Effects of beta-glucans on the immune system, Medicina (Kaunas) 43 (2007) 597–606.
[4] G. Chihara, J. Hamuro, Y.Y. Maeda, T. Shiio, T. Suga, N. Takasuka, T. Sasaki, Antitumor and metastasis-inhibitory activities of lentinan as an immunomodulator: an overview, Cancer Detect Prev. Suppl. 1 (1987) 423–443.
[5] Y. Sakagami, Y. Mizoguchi, T. Shin, S. Seki, K. Kobayashi, S. Morisawa, S. Yamamoto, Effects of an anti-tumor polysaccharide, schizophyllan, on interferon-gamma and interleukin 2 production by peripheral blood mononuclear cells, Biochem. Biophys. Res. Commun. 155 (1988) 650–655.
[6] M. Harada, K. Matsunaga, Y. Oguchi, H. Iijima, K. Tamada, K. Abe, M. Takenoyama, O. Ito, G. Kimura, K. Nomoto, Oral administration of PSK can improve the impaired anti-tumor CD4+ T-cell response in gut-associated lymphoid tissue (GALT) of specific-pathogen-free mice, Int. J. Cancer 70 (1997) 362–372.
[7] F. Hong, J. Yan, J.T. Baran, D.J. Allendorf, R.D. Hansen, G.R. Ostroff, P.X. Xing, N.K. Cheung, G.D. Ross, Mechanism by which orally administered beta-1, 3-glucans enhance the tumoricidal activity of antitumor monoclonal antibodies in murine tumor models, J. Immunol. 173 (2004) 797–806.
[8] F. Hong, R.D. Hansen, J. Yan, D.J. Allendorf, J.T. Baran, G.R. Ostroff, G.D. Ross, Beta-glucan functions as an adjuvant for monoclonal antibody immunotherapy by recruiting tumoricidal granulocytes as killer cells, Cancer Res. 63 (2003) 9023–9031.
[9] M. Fisher, L.X. Yang, Anticancer effects and mechanisms of polysaccharide-K (PSK): implications of cancer immunotherapy, Anticancer Res. 22 (2002) 1737–1754.
[10] K. Oshiman, Y. Fujimiya, T. Ebina, I. Suzuki, M. Noji, Orally administered beta-1, 6-D-polyglucose extracted from *Agaricus blazei* results in tumor regression in tumor-bearing mice, Planta Med. 68 (2002) 610–614.
[11] Q. Dong, J. Yao, X.T. Yang, J.N. Fang, Structural characterization of a water-soluble beta-D-glucan from fruiting bodies of *Agaricus blazei* Murr, Carbohydr. Res. 337 (2002) 1417–1421.
[12] K. Walton, M.M. Coombs, F.S. Catterall, R. Walker, C. Ioannides, Bioactivation of the mushroom hydrazine, agaritine, to intermediates that bind covalently to proteins and induce mutations in the Ames test, Carcinogenesis 18 (1997) 1603–1608.
[13] B. Toth, D. Nagel, Studies of the tumorigenic potential of 4-substituted phenylhydrazines by the subcutaneous route, J. Toxicol. Environ. Health 8 (1981) 1–9.
[14] O. Sterner, R. Bergman, E. Kesler, G. Magnusson, L. Nilsson, B. Wickberg, E. Zimerson, G. Zetterberg, Mutagens in larger fungi: I. Forty-eight species screened for mutagenic activity in the Salmonella/microsome assay, Mutat. Res. 101 (1982) 269–281.
[15] E.G. Rogan, B.A. Walker, R. Gingell, D.L. Nagel, B. Toth, Microbial mutagenicity of selected hydrazines, Mutat. Res. 102 (1982) 413–424.
[16] M. Ishiyama, Y. Miyazono, K. Sasamoto, Y. Ohkura, K. Ueno, A highly water-soluble disulfonated tetrazolium salt as a chromogenic indicator for NADH as well as cell viability, Talanta 44 (1997) 1299–1305.
[17] Y. Oda, H. Yamazaki, M. Watanabe, T. Nohmi, T. Shimada, Development of high sensitive umu test system: rapid detection of genotoxicity of promutagenic aromatic amines by *Salmonella typhimurium* strain NM2009 possessing high *O*-acetyltransferase activity, Mutat. Res. 334 (1995) 145–156.
[18] B. Levenberg, Isolation and structure of agaritine, a gamma-glutamyl-substituted arylhydrazine derivative from Agaricaceae, J. Biol. Chem. 239 (1964) 2267–2273.
[19] L. Wallcave, D.L. Nagel, C.R. Raha, H.-S. Jae, S. Bronczyk, R. Kupper, B. Toth, An improved synthesis of agaritine, J. Org. Chem. 44 (1979) 3752–3755.
[20] A.T. Borchers, J.S. Stern, R.M. Hackman, C.L. Keen, M.E. Gershwin, Mushrooms, tumors, and immunity, Proc. Soc. Exp. Biol. Med. 221 (1999) 281–293.
[21] Y. Fujimiya, Y. Suzuki, K. Oshiman, H. Kobori, K. Moriguchi, H. Nakashima, Y. Matumoto, S. Takahara, T. Ebina, R. Katakura, Selective tumoricidal effect of soluble proteoglucan extracted from the basidiomycete, *Agaricus blazei* Murill, mediated via natural killer cell activation and apoptosis, Cancer Immunol. Immunother. 46 (1998) 147–159.
[22] E. Jimenez-Medina, E. Berruguilla, I. Romero, I. Algarra, A. Collado, F. Garrido, A. Garcia-Lora, The immunomodulator PSK induces in vitro cytotoxic activity in tumour cell lines via arrest of cell cycle and induction of apoptosis, BMC Cancer 8 (2008) 78.
[23] Y. Gu, Y. Fujimiya, Y. Itokawa, M. Oshima, J.S. Choi, T. Miura, T. Ishida, Tumoricidal effects of beta-glucans: mechanisms include both antioxidant activity plus enhanced systemic and topical immunity, Nutr. Cancer 60 (2008) 685–691.
[24] C. Hashida, K. Hayashi, L. Jie, S. Haga, M. Sakurai, H. Shimizu, Quantities of agaritine in mushrooms (*Agaricus bisporus*) and the carcinogenicity of mushroom methanol extracts on the mouse bladder epithelium, Nippon Koshu Eisei Zasshi 37 (1990) 400–405.
[25] K. Pilegaard, E. Kristiansen, O.A. Meyer, J. Gry, Failure of the cultivated mushroom (*Agaricus bisporus*) to induce tumors in the A/J mouse lung tumor model, Cancer Lett. 120 (1997) 79–85.
[26] S.E. Shephard, C. Schlatter, Covalent binding of agaritine to DNA in vivo, Food Chem. Toxicol. 36 (1998) 971–974.
[27] J. Hajslova, L. Hajkova, V. Schulzova, H. Frandsen, J. Gry, H.C. Andersson, Stability of agaritine—a natural toxicant of Agaricus mushrooms, Food Addit. Contam. 19 (2002) 1028–1033.
[28] C. Papaparaskeva, C. Ioannides, R. Walker, Agaritine does not mediate the mutagenicity of the edible mushroom *Agaricus bisporus*, Mutagenesis 6 (1991) 213–217.
[29] C. Papaparaskeva-Petrides, C. Ioannides, R. Walker, Contribution of phenolic and quinonoid structures in the mutagenicity of the edible mushroom *Agaricus bisporus*, Food Chem. Toxicol. 31 (1993) 561–567.
[30] W.N. Gao, D.Q. Wei, Y. Li, H. Gao, W.R. Xu, A.X. Li, K.C. Chou, Agaritine and its derivatives are potential inhibitors against HIV proteases, Med. Chem. 3 (2007) 221–226.

Chemical Physics Letters 490 (2010) 226–229

Contents lists available at ScienceDirect

Chemical Physics Letters

journal homepage: www.elsevier.com/locate/cplett

# Regioselectivity on the cooxidation of 5,6-dihydroxyindole and its 2-carboxy derivative from the quantum chemical calculations

Hidekazu Okuda [a,*], Kazumasa Wakamatsu [b], Shosuke Ito [b], Takayuki Sota [a]

[a] Department of Electrical Engineering and Bioscience, Waseda University, Shinjuku, Tokyo 169-8555, Japan
[b] Department of Chemistry, Fujita Health University School of Health Sciences, Toyoake, Aichi 470-1192, Japan

ARTICLE INFO

*Article history:*
Received 6 October 2009
In final form 18 March 2010
Available online 20 March 2010

ABSTRACT

We report the heterodimerization of eumelanin precursors from the quantum chemical calculations using a general-purpose reactivity indicator. 5,6-Dihydroxyindole (DHI), its 2-carboxy derivative (DHICA), and related molecules are under consideration. Molecules participating in the reaction have been identified from the electron transfer probability. The heterodimerization has been demonstrated to be the electron-transfer-controlled reaction. The theoretical prediction is in good agreement with the result of the previous cooxidation of DHI and DHICA.



## 1. Introduction

Eumelanin is a brown-black macromolecular pigment and is a major component of human pigmentary system. 5,6-Dihydroxyindole (DHI, **1**) and its 2-carboxy derivative (DHICA, **2**) are key eumelanin building blocks [1–8]. The precise polymerization mechanism of them remains unclear. To attack the problem, many experimental efforts have been devoted to isolate oligomers of them [9–16].

Several homooligomers up to tetramers were isolated in the oxidation of **1** or **2** [9,10,12–16]. On the other hand, as for **1**–**2** heterooligomers, the only one oligomer, 5,5′,6,6′-tetrahydroxy-2′-carboxy-2,4′-biindolyl **3**, was isolated from the cooxidation of **1** and **2** [11]. The heteropolymerization mechanism is less understood than homopolymerization although eumelanin is considered to include the heteropolymer of **1** and **2** [1,3,5–8].

Theoretical studies have been already started in the field of eumelanin. **1**-related monomers [17,18], **2**-related monomers [19,20], and their oligomers have been studied [21–28]. The reactivity of **1**-related molecules was recently studied [27] to clarify the oxidative polymerization mechanism of **1** from the quantum chemical calculations using a general-purpose reactivity indicator [29,30]. The theoretical predictions from the quantum chemical calculation-based indicator reasonably explained the structural features of the isolated oligomers of **1**, and so the indicator may be considered useful also for studying the heteropolymerization of **1** and **2**.

In this Letter, we report the reactivity of the tautomers/conformers of **1**- and **2**-related molecules from theoretical point of view to clarify the heterodimerization mechanism of **1** and **2**. It is shown that the energies of the highest occupied molecular orbital (HOMO) and lowest unoccupied molecular orbital (LUMO) of each reactant molecule are associated remarkably with the heterodimerization mechanism: monoionic **1** and neutral **2**-quinone may participate in the heterodimerization, while most of **1** and **2** are considered to exist as neutral and monoionic forms, respectively, in near-neutral solution according to chemical insight.

## 2. Details of calculations

All quantum chemical calculations [31,32] have been carried out using the B3LYP hybrid functional [33], which consists of Becke's exchange functional and the slightly-modified Lee–Yang–Parr correlation functional. The 6-31++$G(d,p)$ basis set [34,35] has been used, which takes account of the d polarization functions on heavy atoms and p polarizations on hydrogen atoms and the diffuse functions for all atoms. The polarizable continuum model [36] has been used for taking the solvent effect into account. The effective point charge on each atom has been estimated by the CHelpG method [37]. Harmonic vibrational wavenumbers have been calculated analytically and scaled by 0.982. Excitation energies of molecules have been estimated using time-dependent density-functional theory (TD-DFT) [38] to evaluate the lowest excitation energy level, i.e., the energy of the LUMO. All quantum chemical calculations have been carried out using the GAUSSIAN03 program [39].

To estimate the reactivity of molecules, the general-purpose reactivity indicator [29,30] has been used. The indicator for nucleophiles is given by

$$\begin{aligned}\Xi^{\kappa}_{\Delta N\leqslant 0.2} &= (\kappa+1)q^{(0)}_{\chi} - \Delta N(\kappa-1)\left[q^{(-)}_{\chi} - q^{(0)}_{\chi}\right] \\ &= (\kappa+1)q^{(0)}_{\chi} - \Delta N(\kappa-1)f^{-}_{\chi},\end{aligned} \tag{1}$$

* Corresponding author. Fax: +81 3 3207 1488.
*E-mail address:* h.okuda@aoni.waseda.jp (H. Okuda).

0009-2614/$ - see front matter © 2010 Elsevier B.V. All rights reserved.
doi:10.1016/j.cplett.2010.03.054

and that for electrophiles is given by

$$\Xi^{\kappa}_{\Delta N\geqslant 0,\alpha} = -(\kappa+1)q^{(0)}_{\alpha} + \Delta N(\kappa-1)\left[q^{(0)}_{\alpha} - q^{(+)}_{\alpha}\right] = -(\kappa+1)q^{(0)}_{\alpha} + \Delta N(\kappa-1)f^{+}_{\alpha}. \quad (2)$$

Here, subscript $\alpha$ specifies the reactive position; $q^{(0)}_{\alpha}$ means the effective point charge on $\alpha$; $q^{(-)}_{\alpha}$ and $q^{(+)}_{\alpha}$ denote the effective point charge on $\alpha$ for the radical cation of the nucleophile without a transferring electron and that for the radical anion of the electrophile with an additional electron, respectively; $f^{\pm}_{\alpha}$ denotes the condensed Fukui functions on $\alpha$ defined as $f^{\pm}_{\alpha} = \pm q^{(0)}_{\alpha} \mp q^{(\pm)}_{\alpha}$. The two parameters, $\Delta N$ and $\kappa$, are also included. $\Delta N$ denotes the amount of electron transfer in the reaction. By varying the value $\kappa$, the indicator covers the entire chemical reactions: strong electrostatic control ($\kappa > 1$), pure electrostatic control ($\kappa = 1$), joint control by electrostatics and electron-transfer effects ($-1 < \kappa < 1$), pure electron-transfer control ($\kappa = -1$), strong electron-transfer control ($\kappa < -1$). The most reactive position of the molecule is the reactive position with the most negative $\Xi^{\kappa}_{\Delta N,\alpha}$. Note that the reactive indices should be estimated with including the adjacent hydrogen atom [29].

In this Letter, the probability of finding each tautomer/conformer has been estimated from the Boltzmann factor ($f_B$), which depends exponentially on both relative energy and temperature:

$$f_{B,i} = \exp\left(-\frac{\Delta G_i}{k_B T}\right), \quad (3)$$

where $\Delta G_i$ means difference of the free energy between the lowest energy molecule and the $i$th tautomer/conformer under consideration; $k_B$ denotes Boltzmann constant; $T$ is absolute temperature. The probability of finding the $i$th tautomer/conformer ($P_i$) is given as

$$P_i = \frac{f_{B,i}}{\sum_j f_{B,j}}. \quad (4)$$

In Eq. (4), $j$ runs over all the tautomers/conformers. Throughout this Letter, $T$ has been set to be 300 K.

As an index of possible reaction, the electron transfer probability between reactants in pH 7.0 has been estimated. The following is the procedure to estimate the electron transfer probability from a nucleophile, B, to an electrophile, A: The energy which an electron should overgo is

$$\Delta\varepsilon_{A,B} = \varepsilon_{LUMO,A} - \varepsilon_{HOMO,B}. \quad (5)$$

Here, $\varepsilon_{LUMO}$ has been estimated from $\varepsilon_{HOMO}$ and the excitation energy:

$$\varepsilon_{LUMO,i} = \varepsilon_{HOMO,i} + E^{ex}_i. \quad (6)$$

The probability of thermal excitation against $\Delta\varepsilon_{A,B}$ is

$$P^{ET}_{\Delta\varepsilon_{A,B}} = \exp\left(-\frac{\Delta\varepsilon_{A,B}}{k_B T}\right). \quad (7)$$

The electron transfer probability between molecules should include the probability of finding each molecule:

$$P^{ET}_{A,B} = P^{ET}_{\Delta\varepsilon_{A,B}} \times (P_A \times R_A) \times (P_B \times R_B), \quad (8)$$

where $P_A \times R_A$ and $P_B \times R_B$ denote the probability of finding A and B, respectively, including the difference between neutral forms and monoionic forms. $P_A$ and $P_B$ are estimated using the Eq. (4); $R_A$ and $R_B$ are estimated from $pK_{an}$:

$$R_A = \begin{cases} 1/(1+10^{4.25-7.0}) & \text{(A is a monoionic form)} \\ 10^{4.25-7.0}/(1+10^{4.25-7.0}) & \text{(A is a neutral form)} \end{cases}, \quad (9)$$

$$R_B = \begin{cases} 1/(1+10^{7.0-9.54}) & \text{(B is a neutral form)} \\ 10^{7.0-9.54}/(1+10^{7.0-9.54}) & \text{(B is a monoionic form)} \end{cases}. \quad (10)$$

Note that $pK_a = 4.25$, 9.76, 13.2 for **2**, $pK_a = 9.54$, 13.14 for **1** [40]. The probability of reactions occurring in units of % should be normalized:

$$P^{react}_{A,B} = \frac{P^{ET}_{A,B}}{\sum_{\alpha\in A}\sum_{\beta\in B} P^{ET}_{\alpha,\beta}} \times 100. \quad (11)$$

Here, $\alpha(\beta)$ runs over all electrophiles (nucleophiles).

## 3. Results and discussion

Molecular structures of **1N**, **1M**, **2N**, and **2M** (Fig. 1) were optimized in aqueous solution. Reasons why they are considered are explained below. The calculated values (bond length, bond angle, excitation energy) for the molecules were compared with the previous results for the related-molecules [17–19,41], validating the present calculations.

The **1**–**2** heterodimer (2,4′-biindolyl, **3**) was isolated in the cooxidation of **1** and **2** [11]. The increase in the yield of the formation of **3** with increasing **1**/**2** ratio suggested that **3** is formed via nucleophilic attacks of **1**-related molecules to **2**-quinones as electrophiles [11]. Therefore, only **1** (**2**)-related molecules were considered here as nucleophiles (electrophiles). It was shown from Hartree–Fock calculations for the monoanions of **2** [41] that the molecule dehydrogenated on the catecholic moiety is energetically preferred in ground state and may explain the absorption and emission spectra of **2**-solution. Thus, the molecules dehydrogenated on catecholic unit, such as **2Mc**, have been also under consideration although carboxylic acids are typically dissociated as $RCOO^-$ anions and $H^+$ cations in neutral solution. Note that the molecules which have no intramolecular hydrogen bond (open forms) are not considered because they are less stable [28]. Previous study demonstrates that $\varepsilon_{HOMO}$ and $\varepsilon_{LUMO}$ for each reactant molecule are significantly important to study the reaction picture [27], and thus, molecules such as **1M** or **2N** should be considered because the molecules have high $\varepsilon_{HOMO}$ or low $\varepsilon_{LUMO}$.

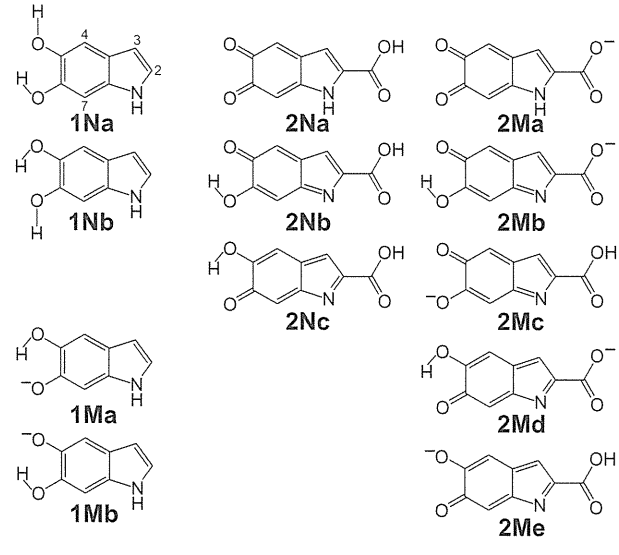


**Fig. 1.** Structural formula of **1N**, **1M**, **2N**, and **2M**. **1** and **2** act as nucleophiles and electrophiles, respectively. The atom-labeling usually used for indoles is also shown for **1Na**. **N** and **M** denote neutral and monoionic forms, respectively.

**Table 1**
Electron transfer probability ($P_{A,B}^{react}$) from a nucleophile to an electrophile in units of %.

| | 2Na | 2Nb | 2Nc | 2Ma | 2Mb | 2Mc | 2Md | 2Me |
|---|---|---|---|---|---|---|---|---|
| **1Na** | $\sim 10^{-14}$ | $\sim 10^{-16}$ | $\sim 10^{-17}$ | $\sim 10^{-16}$ | $\sim 10^{-21}$ | $\sim 10^{-27}$ | $\sim 10^{-21}$ | $\sim 10^{-27}$ |
| **1Nb** | $\sim 10^{-15}$ | $\sim 10^{-17}$ | $\sim 10^{-17}$ | $\sim 10^{-16}$ | $\sim 10^{-22}$ | $\sim 10^{-28}$ | $\sim 10^{-22}$ | $\sim 10^{-28}$ |
| **1Ma** | 94.06 | 1.19 | 0.37 | 4.08 | $\sim 10^{-5}$ | $\sim 10^{-12}$ | $\sim 10^{-5}$ | $\sim 10^{-12}$ |
| **1Mb** | 0.28 | $\sim 10^{-3}$ | $\sim 10^{-3}$ | 0.01 | $\sim 10^{-8}$ | $\sim 10^{-14}$ | $\sim 10^{-8}$ | $\sim 10^{-14}$ |

Since the polymerization of **1** is dominated by the electron-transfer-controlled reaction [27], the electron transfer probability from $\varepsilon_{HOMO,nucl}$ to $\varepsilon_{LUMO,elec}$ has been estimated in order to identify reactants. Results are summarized in Table 1 and suggest that the reaction of **1Ma** against **2Na** is plausible. The effective point charge, the condensed Fukui function, and the reactive indicator on each reactive position for **1Ma** and **2Na** are summarized in Table 2. Here the effective point charge for each reactive position includes that of its adjacent hydrogen atom [29]. Each reactive indicator has been calculated assuming $|\Delta N| = 1$ and $\kappa = -1$ as expected for the heteropolymerization.

In the previous study [27], we have proposed a method how regioselectivity is predicted from the effective point charge and general-purpose reactive indicator. Let us consider the reaction of **1Ma** against **2Na**. Judging from $\Xi^{\kappa=-1}_{|\Delta N|=1,\alpha}$, the C2 position is the most reactive for **1Ma**, while the C4 position is the most reactive for **2Na**. The effective point charge on the C2 position of **1Ma** is considered small enough not to prevent the formation of the C2–C4 bond between **1Ma** and **2Na**. Indeed, when the radical ion picture is used, the strongest Coulomb attraction acts between the C2 position of **1Ma** and the C4 position of **2Na**. Thus, 2,4′-biindolyl (**3**) may be formed via the reaction.

The present theory predicts **3** as a primary product of the cooxidation of **1** and **2** in accordance with the previous experimental result [11]. The formation scheme of **3** is shown in Fig. 2. The previous study [11] has reported one more heterooligomer in addition to **3**. However, to the best of our knowledge, its formula has not been experimentally identified, yet. Table 2 suggests that the unknown heterooligomer is 2,7′-biindolyl as a secondary product from the reaction of **1Ma** against **2Na**. Note that the reactivity of the C3 position of **2Na** is negligibly-small (Table 2). 2,7′-Biindolyl may be formed also via the reaction of **1Ma** against **2Ma**, the next plausible reaction (Table 1). It is because the C7 position is the most reactive position among the reactive positions of **2Ma** (not shown).

In this Letter, we have estimated the electron transfer probability using the lowest excitation energy within TD-DFT. This is validated from the two following reasons. First, TD-DFT is widely known to have enough accuracy for the excitation energy [42]. Indeed, the recent theoretical studies in the field of eumelanin have often used the method [17,22–26,28]. Second, the order of the electron transfer probability is important in this Letter. So the accuracy demanded about probability is not so high.

**Table 2**
Effective point charge, condensed Fukui function, and reactive indicator for each reactive position of **1Ma** and **2Na**. For the labels of the atoms, see Fig. 1.

| | | C2 | C3 | C4 | C7 |
|---|---|---|---|---|---|
| **1Ma** | $q_\alpha^{(0)}$ | −0.0164 | −0.1670 | −0.2697 | −0.3186 |
| | $q_\alpha^{(-)}$ | 0.1760 | −0.1342 | −0.2223 | −0.1862 |
| | $f_\alpha^-$ | 0.1925 | 0.0328 | 0.0474 | 0.1324 |
| | $\Xi^{\kappa=-1}_{\Delta N=-1,\alpha}$ | −0.3849 | −0.0657 | −0.0947 | −0.2647 |
| **2Na** | $q_\alpha^{(0)}$ | | −0.0746 | −0.2110 | −0.2369 |
| | $q_\alpha^{(+)}$ | | −0.0899 | −0.3296 | −0.3104 |
| | $f_\alpha^+$ | | 0.0152 | 0.1185 | 0.0735 |
| | $\Xi^{\kappa=-1}_{\Delta N=1,\alpha}$ | | −0.0305 | −0.2371 | −0.1470 |

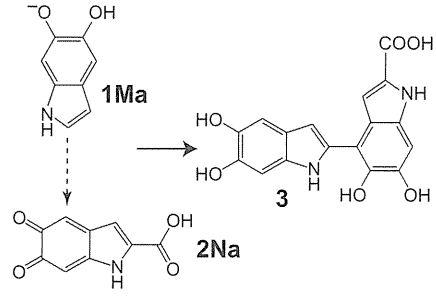


**Fig. 2.** Reaction scheme of formation of **3** from the theoretical prediction. The nucleophilic attack of the C2 position for **1Ma** to the C4 position for **2Na** leads to **3**.

In summary we have studied the cooxidation of DHI and DHICA from the quantum chemical calculations using the general-purpose reactive indicator. The theoretical prediction has agreed with the previous experimental results. The cooxidation of DHI and DHICA has been suggested to be the electron-transfer-controlled reaction. Which molecule participates in the reaction has been identified from the electron transfer probability.

## References

[1] S. Ito, Pigment Cell Res. 16 (2003) 230.
[2] M. d'Ischia, A. Napolitano, A. Pezzella, E.J. Land, C.A. Ramsden, P.A. Riley, Adv. Heterocycl. Chem. 89 (2005) 1.
[3] P. Meredith, B.J. Powell, J. Riesz, S.P. Nighswander-Rempel, M.R. Pederson, E.G. Moore, Soft Matter 2 (2006) 37.
[4] P. Meredith, T. Sarna, Pigment Cell Res. 19 (2006) 572.
[5] S. Ito, K. Wakamatsu, Photochem. Photobiol. 84 (2008) 582.
[6] J.D. Simon, L. Hong, D.N. Peles, J. Phys. Chem. B 112 (2008) 13201.
[7] J.D. Simon, D. Peles, K. Wakamatsu, S. Ito, Pigment Cell Melanoma Res. 22 (2009) 563.
[8] M. d'Ischia, A. Napolitano, A. Pezzella, P. Meredith, T. Sarna, Angew. Chem. Int. Ed. 48 (2009) 3914.
[9] A. Napolitano, M.G. Corradini, G. Prota, Tetrahedron Lett. 26 (1985) 2805.
[10] M. d'Ischia, A. Napolitano, K. Tsiakas, G. Prota, Tetrahedron 46 (1990) 5789.
[11] A. Napolitano, O. Crescenzi, G. Prota, Tetrahedron Lett. 34 (1993) 885.
[12] A. Pezzella, A. Napolitano, M. d'Ischia, G. Prota, Tetrahedron 52 (1996) 7913.
[13] A. Pezzella, D. Vogna, G. Prota, Tetrahedron 58 (2002) 3681.
[14] A. Pezzella, D. Vogna, G. Prota, Tetrahedron: Asymmetry 14 (2003) 1133.
[15] L. Panzella, A. Pezzella, A. Napolitano, M. d'Ischia, Org. Lett. 9 (2007) 1411.
[16] A. Pezzella, L. Panzella, A. Natangelo, M. Arzillo, A. Napolitano, M. d'Ischia, J. Org. Chem. 72 (2007) 9225.
[17] Y.V. Il'ichev, J.D. Simon, J. Phys. Chem. B 107 (2003) 7162.
[18] B.J. Powell, T. Baruah, N. Bernstein, K. Brake, R.H. McKenzie, P. Meredith, M.R. Pederson, J. Chem. Phys. 120 (2004) 8608.
[19] B.J. Powell, Chem. Phys. Lett. 402 (2005) 111.
[20] H. Okuda, A. Nakamura, K. Wakamatsu, S. Ito, T. Sota, Chem. Phys. Lett. 433 (2007) 355.
[21] M.L. Tran, B.J. Powell, P. Meredith, Biophys. J. 90 (2006) 743.
[22] E. Kaxiras, A. Tsolakidis, G. Zonios, S. Meng, Phys. Rev. Lett. 97 (2006) 218102.
[23] A. Pezzella et al., J. Am. Chem. Soc. 128 (2006) 15490.
[24] S. Meng, E. Kaxiras, Biophys. J. 94 (2008) 2095.
[25] S. Meng, E. Kaxiras, Biophys. J. 95 (2008) 4396.
[26] M. d'Ischia, O. Crescenzi, A. Pezzella, M. Arzillo, L. Panzella, A. Napolitano, V. Barone, Photochem. Photobiol. 84 (2008) 600.
[27] H. Okuda, K. Wakamatsu, S. Ito, T. Sota, J. Phys. Chem. A 112 (2008) 11213.

[28] A. Pezzella et al., J. Org. Chem. 74 (2009) 3727.
[29] J.S.M. Anderson, J. Melin, P.W. Ayers, J. Chem. Theory Comput. 3 (2007) 358.
[30] J.S.M. Anderson, J. Melin, P.W. Ayers, J. Chem. Theory Comput. 3 (2007) 375.
[31] R.G. Parr, W. Yang, Density-Functional Theory of Atoms and Molecules, Oxford University Press, New York, 1989.
[32] W. Koch, M.C. Holthausen, A Chemist's Guide to Density Functional Theory, second edn., Wiley-VCH, Weinheim, 2001.
[33] A.D. Becke, J. Chem. Phys. 98 (1993) 5648.
[34] G.A. Petersson, A. Bennett, T.G. Tensfeldt, M.A. Al-Laham, W.A. Shirley, J. Mantzaris, J. Chem. Phys. 89 (1988) 2193.
[35] T. Clark, J. Chandrasekhar, G.W. Spitznagel, P.V.R. Schleyer, J. Comput. Chem. 4 (1983) 294.
[36] R. Cammi, B. Mennucci, J. Tomasi, J. Phys. Chem. A 104 (2000) 5631.
[37] C.M. Breneman, K.B. Wiberg, J. Comput. Chem. 11 (1990) 361.
[38] E. Runge, E.K.U. Gross, Phys. Rev. Lett. 52 (1984) 997.
[39] M.J. Frisch et al., GAUSSIAN03, Revision D.02, Gaussian Inc., Wallingford CT, 2004.
[40] L.K. Charkoudian, K.J. Franz, Inorg. Chem. 45 (2006) 3657.
[41] S. Olsen et al., J. Am. Chem. Soc. 129 (2007) 6672.
[42] M. Orio, D.A. Pantazis, F. Neese, Photosynth. Res. 102 (2009) 443.

THE JOURNAL OF IMMUNOLOGY



# Spatiotemporal Regulation of Heat Shock Protein 90-Chaperoned Self-DNA and CpG-Oligodeoxynucleotide for Type I IFN Induction via Targeting to Static Early Endosome

Koichi Okuya, Yasuaki Tamura, Keita Saito, Goro Kutomi, Toshihiko Torigoe, Koichi Hirata and Noriyuki Sato

*J Immunol* 2010;184;7092-7099; Prepublished online 14 May 2010;
doi:10.4049/jimmunol.1000490
http://www.jimmunol.org/content/184/12/7092



*The Journal of Immunology* is published twice each month by
The American Association of Immunologists, Inc.,
9650 Rockville Pike, Bethesda, MD 20814-3994.

Print ISSN: 0022-1767 Online ISSN: 1550-6606.

# Spatiotemporal Regulation of Heat Shock Protein 90-Chaperoned Self-DNA and CpG-Oligodeoxynucleotide for Type I IFN Induction via Targeting to Static Early Endosome

Koichi Okuya,*,† Yasuaki Tamura,* Keita Saito,*,† Goro Kutomi,† Toshihiko Torigoe,* Koichi Hirata,† and Noriyuki Sato*

**Recent studies have suggested that TLR9 signaling in early endosomes leads to IFN-α production by plasmacytoid dendritic cells (pDCs), whereas TLR9 signaling in late endosomes induces pDC maturation, IL-6, and TNF-α secretion. In this study, we show that human DNA as well as CpG-oligodeoxynucleotides (ODNs) in complex with heat shock protein 90 (Hsp90) stimulate pDCs to produce large quantities of IFN-α. The Hsp90–CpG-A complexes are targeted into the Rab5$^+$, early endosomal Ag 1$^+$-static early endosome postinternalization by DCs, suggesting that preferential sorting of Hsp90-chaperoned self-DNA/CpG-ODNs to the static endosome is required for signaling through TLR9 for IFN-α production. Interestingly, Hsp90-mediated preferential static early endosomal translocation of CpG-ODNs triggers robust IFN-α production from murine conventional DCs. Thus, extracellular Hsp90 converts inert self-DNA/CpG-ODNs into a potent trigger of IFN-α production via spatiotemporal regulation.** ***The Journal of Immunology*****, 2010, 184: 7092–7099.**

Heat shock proteins (HSPs) are molecular chaperones that control the folding and prevent the aggregation of proteins. It is well known that tumor-derived HSPs, such as Hsp70, Hsp90, and gp96, initiate efficient tumor-specific CTL responses and protective immunity (1–6). We have demonstrated that extracellular HSP–Ag peptide complexes are efficiently cross-presented via the endosome–recycling pathway (7, 8). In this HSP-mediated cross-presentation, the receptor-dependent endocytosed HSP–peptide complex is translocated to the early endosome, and thereafter, the Hsp90-chaperoned peptide is transferred onto recycling MHC class I molecules.

Bacterial and viral DNAs rich in CpG motifs or small synthetic oligodeoxynucleotides (ODNs) containing CpG motifs activate innate immune cells, such as dendritic cells (DCs), via TLR9 (9, 10). TLR9 is expressed within endolysosomal compartments in innate immune cells and recognizes distinct patterns of nucleic acids in the endolysosomal compartments (11–15). Upon TLR9 engagement, IFN-α induction depends on the MyD88–IFN regulatory factor (IRF)-7 signaling pathway (16, 17). DC subpopulations are characterized by expression of different surface markers and the ability to produce cytokines that modulates both innate resistance and the adaptive immune response (18). In the murine system, the plasmacytoid DCs (pDCs) are CD11c$^{low}$ B220$^{high}$ Ly6C$^{high}$ cells exhibiting plasmacytoid morphology and are able to produce a high level of IFN-α in response to several viruses or to CpG-ODN (19–21). Murine CD11c$^{high}$ conventional DCs (cDCs) have been further subdivided into subsets, such as CD8$^+$ DCs and CD8$^-$ DCs (18). In humans, CD11c$^-$ IL-3R$^{high}$ pDCs differ from CD11c$^+$ myeloid DCs (mDCs) in being uniquely able to produce a large amount of IFN-α in response to viral stimulation (22, 23) or to CpG-ODN (24). Previous studies revealed that CpG-A or various DNAs needed to be retained for long periods in the endosomes of pDCs for sufficient activation of TLR9 signaling (25, 26). Recently, CpG-ODNs have shown promising results as vaccine adjuvants for cancer immunotherapy due to their ability to induce potent Th1-type immune responses and anti-tumor responses (27–30).

Very recently, Lakadamyali et al. (31) have shown that early endosomes are comprised of two distinct populations called static early endosomes, which are slow maturing, and rapidly maturing dynamic early endosomes.

We have demonstrated that targeting of HSP–peptide complexes to the early endosomal Ag 1 (EEA1)$^+$, Rab5$^+$-static early endosome is crucial for cross-presentation (8).

In this study, we show that Hsp90 can form complexes with CpG-ODNs in vitro and that these complexes act as potent inducers of IFN-α production not only by pDCs but also cDCs. Furthermore, we show that extracellular CpG-ODN–Hsp90 complexes accumulate in the static early endosome but not the dynamic early endosome when pulsed onto DCs. In the human system, Hsp90 can convert inert self-DNA into a potent trigger of IFN-α production by targeting static early endosomes via spatiotemporal regulation. Thus, extracellular Hsp90 can be an excellent immunomodulator for cancer immunotherapy via spatiotemporal regulation of chaperoned molecules.

## Materials and Methods

### *Mice*

C57BL/6 mice were obtained from The Jackson Laboratory (Bar Harbor, ME). *Tlr9*$^{-/-}$ mice were kindly provided by Dr. S. Akira (Osaka University, Osaka, Japan). All mice were kept in a specific-pathogen-free

*Department of Pathology and †Department of Surgery, Sapporo Medical University School of Medicine, Sapporo, Japan

Received for publication February 12, 2010. Accepted for publication April 14, 2010.

This work was supported in part by Grant-in-Aid for Scientific Research and Program for developing the supporting system for upgrading the education and research from the Ministry of Education, Culture, Sports, Science and Technology and Health and Labor Sciences Research Grant-in Aid from the Ministry of Health, Labor, and Welfare of Japan.

Address correspondence and reprint requests to Dr. Yasuaki Tamura, Sapporo Medical University School of Medicine, S1W17, Chuo-ku, Sapporo, Hokkaido 060-8556, Japan. E-mail address: ytamura@sapmed.ac.jp

The online version of this article contains supplemental material.

Abbreviations used in this paper: cDC, conventional dendritic cell; DC, dendritic cell; EEA1, early endosomal Ag 1; ER, endoplasmic reticulum; HSP, heat shock protein; IRF, IFN regulatory factor; LAMP1, lysosome-associated membrane protein 1; mDC, myeloid DC; ND, not detected; NS, normal saline; ODN, oligodeoxynucleotide; pDC, plasmacytoid dendritic cell; SLE, systemic lupus erythematosus.



www.jimmunol.org/cgi/doi/10.4049/jimmunol.1000490

mouse facility. Studies were performed by an approval of Animal Experiment Ethics Committee of Sapporo Medical University (Sapporo, Japan).

### *Oligodeoxynucleotides*

Synthesized CpG ODNs were purchased from Sigma-Aldrich (St. Louis, MO) and Invivogen (San Diego, CA). The sequences of ODNs were: murine CpG-A, 5′-ggTGCATCGATGCAgggggG-3′; murine CpG-B, 5′-tccatgacgttcctgatgct-3′; and control CpG ODN, 5′-ggTGCATGCATGCAgggggg-3′. ODN2216 was CpG ODN type A-human TLR9 ligand (5′-ggGGGACGATCGTCgggggg-3′) and purchased from Invivogen.

### *Protein and Abs*

Purified human Hsp90 was purchased from Stressgen (Ann Arbor, MI). Organelles were detected by laser confocal microscopy with specific Abs against KDEL (Stressgen) for endoplasmic reticulum (ER), Rab5 (Santa Cruz Biotechnology, Santa Cruz, CA) and EEA1 (Abcam, Cambridge, MA) for early endosomes, and lysosome-associated membrane protein 1 (LAMP1) (Santa Cruz Biotechnology) for lysosomes. Each Ab was labeled with Alexa Fluor 488 or Alexa Fluor 594 (Molecular Probes, Eugene, OR). Alexa Fluor 488 was used for labeling Hsp90.

### *Preparation of DCs*

Murine cDCs and pDCs were isolated from bone marrow-derived DCs using magnetic beads and the MACS system (Miltenyi Biotec, Auburn, CA). Bone marrow cells were cultured for 5 d in a 5% $CO_2$ environment at 37°C in complete RPMI 1640 medium with 10% FCS, 20 ng/ml GM-CSF (Endogen, Woburn, MA), and 50 μM 2-ME (Invitrogen, Carlsbad, CA). Murine pDCs were purified using a Plasmacytoid Dendritic Cell Isolation Kit (Miltenyi Biotec), and cDCs were purified by negative selection with anti-murine pDC Ag 1 microbeads (Miltenyi Biotec), followed by positive selection with CD11c beads (Miltenyi Biotec). To confirm the expression of TLR9 and IRF7, pDCs and cDCs were lysed with 0.5% CHAPS containing protease inhibitor (Roche, Basel, Switzerland). Equal amounts of protein were separated by SDS-PAGE and analyzed by immunoblotting with anti-TLR9 (Invivogen), anti-IRF7 (Abcam), and β-actin Abs (Sigma-Aldrich). For RT-PCR, RNA was isolated from pDCs and mouse spleen cells using an RNeasy mini kit (Qiagen, Valencia, CA). Cells were pelleted at 4°C and resuspended in RLT lysis buffer (Qiagen). Total RNA was extracted following on-column DNase digestion using RNeasy mini columns and collected in RNase-free water. Oligo(dT)-primed reverse transcriptase of RNA into cDNA was performed with a Superscript III first-strand synthesis kit (Invitrogen), and 5% of the product was used for each RT-PCR sample using PCR buffer with hot-start Invitrogen Taq polymerase (Invitrogen). Primer pairs for TLR9 (forward 5′-GCTTTGGCCTTTCACTCTTG-3′ and reverse 5′-AACTGCGCTCTGTGCCTTAT-3′) and GAPDH (forward 5′-GAGTCAACGGATTTGGTCGT-3′ and reverse 5′-TTGATTTTGGAGGGATCTCG-3′) were designed using Primer3. Human mDCs and pDCs were isolated from PBMCs of healthy donors with mDC and pDC isolation kits (Miltenyi Biotec) according to the manufacturer's instructions.

### *Generation of CpG-ODN–Hsp90 complex in vitro*

To confirm whether CpG-ODN–Hsp90 complexes could be generated, 1.5 nmol CpG-ODN was end labeled with T4-polynucleotide kinase and γ[$^{32}$P]-ATP, followed by incubation with 0.5 μM purified Hsp90 (Stressgen) at 37°C for 30 min. These samples were then separated by native-PAGE, and the gels were analyzed with silver staining and exposed to a Fuji BAS-MS imaging plate (Fuji Medical Systems, Tokyo, Japan) for ~24 h. The images were scanned using a BAS-2500 Phosphor Imaging System (Fuji Medical Systems). To make 3 μM CpG-ODN–Hsp90 complex, 3 nmol CpG-ODN was mixed with 1 μM Hsp90, incubated for 30 min, and then diluted with 1 ml medium.

### *Measurement of cytokine production*

DCs were plated at 5–10 × $10^4$ cells/well in flat-bottomed, 96-well plates in 100 μl complete RPMI 1640 medium with 10% FCS and stimulated with various reagents for 24 h. CpG–ODN or CpG-ODN–Hsp90 complex was added to medium at a final concentration of 3 μM. Supernatants were diluted and tested for various cytokines with mouse or human IFN-α (PBL InterferonSource, Piscataway, NJ), TNF-α (Pierce, Rockford, IL), and IL-6 (R&D Systems, Minneapolis, MN) using a sandwich ELISA kit. Absorbance was determined at 450 nm.

### *Flow cytometry*

For detection of cell surface-bound and intracellular CpG-A that was transported by cDC and pDC, isolated mouse cDCs and pDCs were incubated with synthesized Cy5-labeled CpG-A (Sigma-Aldrich) or a complex with Hsp90 at 37°C. After 30 min, flow cytometric analysis was performed on an FACSCaliber flow cytometer (BD Biosciences, San Jose, CA).

### *Confocal imaging*

Hsp90 was conjugated with Alexa Fluor 488 (Molecular Probes) according to the manufacturer's instructions. To visualize the kinetics of exogenously loaded Hsp90, purified cDCs were seeded on glass coverslips for 12 h and were first incubated with Alexa Fluor 488-labeled Hsp90 (10 μg) at 4°C for 10 min and washed. The cells were then further incubated for 0–120 min, fixed with 4% paraformaldehyde for 5 min at room temperature, and visualized. For the detection of colocalization with exogenous Hsp90 and organelles, cDCs were incubated with Alexa Fluor 488-labeled Hsp90 at 37°C for 120 min and washed. The cells were then fixed with 4% paraformaldehyde, permeabilized with 0.1% Triton X-100, and then blocked with 10% goat serum for 40 min. Cells were stained with anti-KDEL for detecting ER, anti-LAMP1 for late endosomes and lysosomes, and anti-Rab5 and anti-EEA1 for early endosomes for 60 min, followed by Alexa Fluor 594-conjugated goat anti-rabbit IgG for 60 min, and mounted. To analyze the intracellular routing of CpG-A, cDCs were seeded on glass coverslips for 12 h and stimulated with Cy5-labeled CpG-A alone for 30 min. Then the cells were washed and incubated with medium without CpG-A for 0, 60, and 120 min, fixed, permeabilized with 0.1% Triton X-100, and blocked with 10% goat serum for 40 min. Following this, they were stained with anti-EEA1 and anti-LAMP1 Abs followed by Alexa Fluor 488-conjugated goat anti-rabbit IgG. To analyze the intracellular routing of complexed CpG-A with Hsp90, cDCs were seeded on glass coverslips for 12 h and stimulated with complexed Cy5-labeled CpG-A with Hsp90 for 30 min. Then the cells were washed and incubated with medium without CpG-A for 0, 60 and 120 min, fixed with 4% paraformaldehyde, permeabilized with 0.1% Triton X-100 and blocked with 10% goat serum for 40 min. Following this, they were stained with anti-Rab5, anti-EEA1, and anti-LAMP1 Abs followed by Alexa Fluor 488-conjugated goat anti-rabbit IgG. All samples were visualized using an LSM510 confocal microscope (Zeiss, Oberkochen, Germany), and images were captured and analyzed using the Zeiss LSM Image Browser (Zeiss). For evaluation of colocalization, a single *z*-plane of one cell was evaluated. For each protein and organelle combination, a total of 150 cells (50 cells each from three independent experiments) were analyzed.

### *Mouse injections*

For analysis of in vivo cytokine production induced by stimulation with CpG-A, C57BL/6 mice were anesthetized and challenged with normal saline (50 μl), Hsp90 (20 μg/mouse), CpG-A (50 μg/mouse), and CpG-A (50 μg) complexed with Hsp90 (20 μg) by the i.p. route. After 12 h, blood was collected by cardiac puncture, and serum was prepared for IFN-α ELISA. Spleens were collected and crushed for isolation of spleen cells, and cDCs were enriched by negative selection using anti-murine pDC Ag 1 microbeads, followed by positive selection using anti-CD11c microbeads, and cultured for 24 h. Supernatants were then collected for IFN-α ELISA.

### *Genomic DNA isolation*

Human genomic DNA was isolated from PBMCs of healthy donors using a DNeasy kit (Qiagen) according to the manufacturer's instructions.

### *Statistical analysis*

All experiments were independently performed three times in triplicate. Results were given as means + SEM. Comparisons between two groups were performed using Student *t* test, whereas comparisons among multiple groups were done using ANOVA, with a value of $p < 0.05$ considered to be statistically significant.

## Results

### *Extracellulary loaded Hsp90 accumulates in static early endosomes within cDCs*

We first examined the intracellular trafficking of extracellular Hsp90 loaded onto cDCs. We labeled native Hsp90 protein with Alexa Fluor 488 and loaded it onto cDCs separated from mouse bone marrow-derived DCs using an anti-CD11c Ab at 4°C for 10 min and washed. The cells were then further incubated for 0–120 min, and we analyzed the kinetics of intracellular trafficking of Hsp90. Extracellular Hsp90 was gradually trafficked from the cell surface to the cytosol with the passage of time (Fig. 1*A*). To

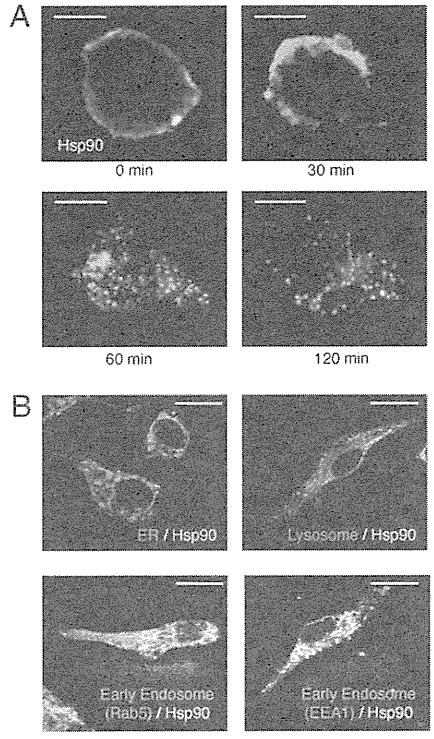


**FIGURE 1.** Extracellulary loaded Hsp90 accumulates in the static early endosome. *A*, Isolated murine cDCs were loaded with Alexa Fluor 488-labeled Hsp90 (10 μg) at 4°C for 10 min and washed. The cells were then further incubated for 0–120 min and fixed with 4% paraformaldehyde, and then visualized by laser confocal microscopy (original magnification ×630). Bar, 5 μm. *B*, Isolated cDCs were pulsed with Alexa Fluor 488-labeled Hsp90 for 2 h. Postincubation, the cells were fixed and stained with anti-KDEL (for ER), anti-LAMP1 (for late endosomes and lysosomes), anti-Rab5 (for early endosomes), and anti-EEA1 (for static early endosomes) followed by Alexa Fluor 594-conjugated goat anti-rabbit IgG or anti-mouse IgG, and then visualized by laser confocal microscopy (original magnification ×630). Bar, 10 μm. Data in *A* and *B* are representative of three independent experiments.

investigate the intracellular localization of extracellular Hsp90, cDCs were incubated with the Alexa Fluor 488-labeled Hsp90 for 30 min and washed. Postincubation with medium without Hsp90 for 120 min, the cells were fixed and stained with organelle markers, such as KDEL for ER, LAMP1 for the late endosome and lysosome, and Rab5 and EEA1 for the early endosome. Extracellular Hsp90 accumulated in Rab5 and EEA1 positive-early endosomes but not in ER or late endosomes/lysosomes (Fig. 1*B*). These results indicated that extracellular Hsp90 was sorted into the static early endosomal pathway and retained for longer periods, but not the dynamic early endosomal pathway. These observations led us to investigate whether extracellular Hsp90 converted non–IFN-α stimulatory CpG-A ODN into a trigger of cDC activation to produce IFN-α.

*In vitro generation of CpG-ODN–Hsp90 complex*

As Hsp90 has been demonstrated to be a binder to CpG-ODNs (32), we first confirmed whether Hsp90 could be complexed with CpG-A and control CpG in vitro. We incubated 1.5 nmol end labeled CpG-ODN with 0.5 μM Hsp90 at 37°C for 30 min. Samples were subjected to native-PAGE and visualized by silver staining (Fig. 2*A*) and autoradiograpy (Fig. 2*B*). These results indicated that Hsp90 could bind CpG-ODNs. To make a 3 μM CpG-ODN–Hsp90 complex, 3 nmol CpG-A or CpG-B was mixed with 1 μM Hsp90, incubated for 30 min, and then diluted with 1 ml medium.

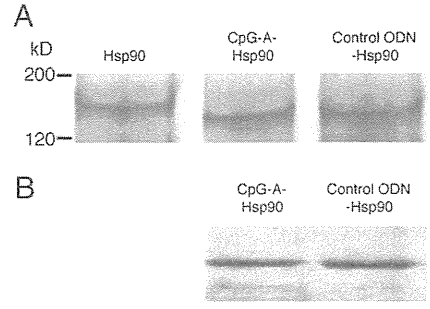


**FIGURE 2.** In vitro generation of CpG-ODN–Hsp90 complex. Purified Hsp90 (0.5 μM) and CpG-DNA (1.5 nmol) that were end labeled with T4-polynucleotide kinase and (γ[$^{32}$P])-ATP were incubated at 37°C for 30 min. Samples were separated by native-PAGE. *A*, The gels were analyzed using silver staining. *B*, The gels were exposed to a Fuji BAS-MS imaging plate (Fuji Medical Systems) for 24 h, and the images were scanned using the Phosphor Imaging System (Fuji Medical Systems).

*Hsp90 enhances IFN-α induction in response to CpG-A from pDC and cDC*

Mouse pDCs, not cDCs, have previously been demonstrated to be the major cells secreting IFN-α following CpG-A stimulation. To elucidate the ability of Hsp90 to enhance secretion of IFN-α from the DC subset, freshly isolated pDCs were cultured for 24 h in the presence of 3 μM CpG-A or 3 μM CpG-A–Hsp90 complex, respectively. The CpG-A–Hsp90 complex enhanced the IFN-α production 2-fold more than CpG-A alone (Fig. 3*A*). Notably, a high amount of IFN-α production was observed in cDCs stimulated with the CpG-A–Hsp90 complex despite the lack of production of IFN-α

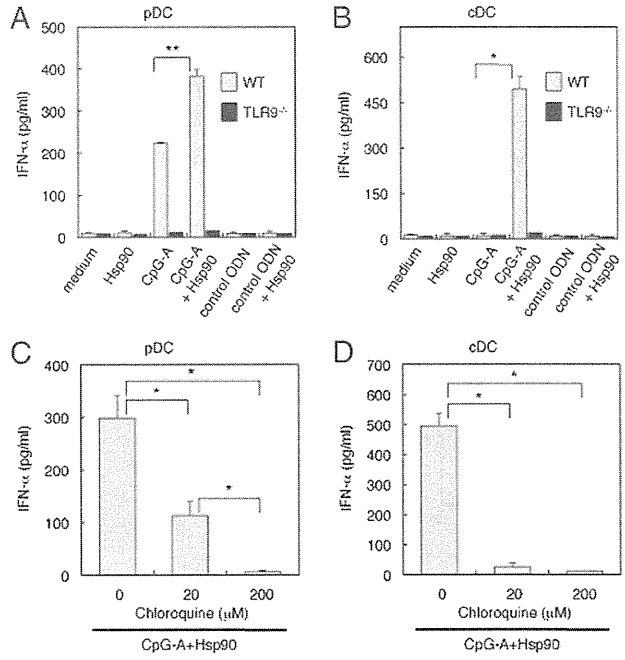


**FIGURE 3.** CpG-A–Hsp90 complexes enhance induction of IFN-α by DCs in vitro. IFN-α production poststimulation with 3 μM CpG-A, control ODN alone, or in complex with Hsp90 by pDCs from WT and *Tlr9*$^{-/-}$ mice (*A*) and cDCs from WT and *Tlr9*$^{-/-}$ mice (*B*). The effect of chloroquine treatment on IFN-α production poststimulation with 3 μM CpG-A–Hsp90 complex by pDCs (*C*) and cDCs (*D*). IFN-α production was determined by ELISA. Data are presented as means + SEM of triplicate wells. Data are representative of three independent experiments. $*p < 0.0005$; $**p < 0.001$, paired Student *t* test.

when they were stimulated with CpG-A alone (Fig. 3*B*). Exogenous Hsp90 did not have any effect on IFN-α secretion by either pDCs or cDCs (Fig. 3*A*, 3*B*). Furthermore, the observed IFN-α production was completely inhibited poststimulation with the CpG-A–Hsp90 complex in both pDCs and cDCs derived from *Tlr9*$^{-/-}$ mice (Fig. 3*A*, 3*B*). Moreover, IFN-α production was potently inhibited by chloroquine, which blocks endosomal signaling (Fig. 3*C*, 3*D*). The degree of the inhibition of the IFN-α production by chloroquine was different between pDCs and cDCs, but this may have been due to the sensitivity to the chloroquine. These results suggested that Hsp90 might translocate the chaperoned CpG-ODNs into static early endosomes and efficiently activate the TLR9 signaling pathway for IFN-α production.

*Both cDCs and pDCs uptake CpG-A to similar degrees*

We compared the efficiency of binding and uptake of CpG-A or the CpG-A–Hsp90 complex by cDCs and pDCs to rule out the possibility that Hsp90 enhanced the uptake of CpG-A by cDCs and pDCs. Cy5-labeled CpG-A, either coupled with Hsp90 or alone, was added to cDC or pDC cultures, and the binding and uptake were analyzed. The percentage of cDCs that took-up CpG-A was 36.9% with CpG-A stimulation alone, and it was approximately the same, 39.5%, when it was coupled with Hsp90 (Fig. 4). The uptakes of CpG-A alone and the CpG-A–Hsp90 complex by pDCs were also similar. These results indicated that both cDCs and pDCs took up the labeled CpG-ODN at almost the same level and supported our hypothesis that Hsp90-mediated direction of CpG-A into the early endosome might be essential for IFN-α production in cDCs.

*Mouse cDCs express TLR9 and IRF7*

We examined whether TLR9 was expressed by murine cDCs. TLR9 protein and mRNA expression were determined by immunoblot and RT-PCR analyses using freshly isolated highly purified cDCs populations (Supplemental Fig. 1*A*, 1*B*). Laser confocal microscopic analysis revealed that TLR9 localized in the EEA1-positive early endosomes of cDCs (Supplemental Fig. 1*C*).

*CpG-ODN–Hsp90 complex serves as a potent inducer for IFN-α in vivo*

Next, we examined whether the CpG-A–Hsp90 complex had an in vivo effect similar to that observed in vitro. We administered PBS, Hsp90 alone, CpG-A alone, or the CpG-A–Hsp90 complex to C57BL/6 mice. After 12 h, we collected sera from the mice and measured the IFN-α. The production of IFN-α from mice injected with the CpG-A–Hsp90 complex was higher than that induced by CpG-A alone (Fig. 5*A*). Moreover, production of IFN-α by cDCs isolated from spleens of treated mice and cultured ex vivo for 40 h was measured. cDCs isolated from mice injected with the CpG-A–Hsp90 complex produced a high level of IFN-α. In contrast, cDCs from mice injected with CpG-A alone did not (Fig. 5*B*). These results indicated that Hsp90 could target chaperoned molecules to the early endosomal compartment within cDCs and induce robust INF-α secretion in vivo as well as in vitro.

*Hsp90 retains CpG-ODN in static early endosomes*

We assumed that in cDCs, as CpG-A was rapidly trafficked to late endosomes and lysosomes, CpG-A–mediated TLR9 signaling was not sufficient. We therefore investigated the intracellular routing of CpG-A after uptake of it in cDCs using laser confocal microscopy. Isolated cDCs from BMDCs were incubated with Cy5-labeld CpG-A for 30 min, and then the cells were washed and incubated with new medium without CpG-A for 0, 60, and 120 min. Following incubation, the cells were fixed and stained. Immediately poststimulation, most of the CpG-A localized within LAMP1$^+$ late endosomes/lysosomes (Fig. 6*A*, Supplemental Fig. 2). In contrast, the frequency of colocalization with EEA1 was very low. After 120 min incubation, CpG-A was detected within late endosmes/lysosomes at high frequency and in a large area of the LAMP1$^+$ organelle (Fig. 6*A*, Supplemental Fig. 2). Together with our observation that TLR9 localized in the EEA1 positive-early endosomes of cDCs, these results indicated that CpG-A was rapidly trafficked to the LAMP1$^+$ late endosme/lysosome pathway, and therefore could not activate the TLR9–MyD88–IRF7 signaling pathway. In contrast, Cy5-labeled CpG-A coupled with Hsp90 was pooled for at least 120 min during stimulation within Rab5$^+$, EEA1$^+$-static early endosomes, and lysosomal localization was poorly detected (Fig. 6*B*, Supplemental Fig. 3). Furthermore, when complexed with Hsp90, CpG-A appeared to form large aggregates that colocalized with early endosomes after 120 min (Fig. 6*B*). These results suggested that their ability to form aggregated structures was needed to induce IFN-α. Quantitative analysis of the colocalization between the Cy5-labeled CpG-A and EEA1 and LAMP1 revealed average colocalization incidences of 16.7% and 91.9%, respectively, immediately after

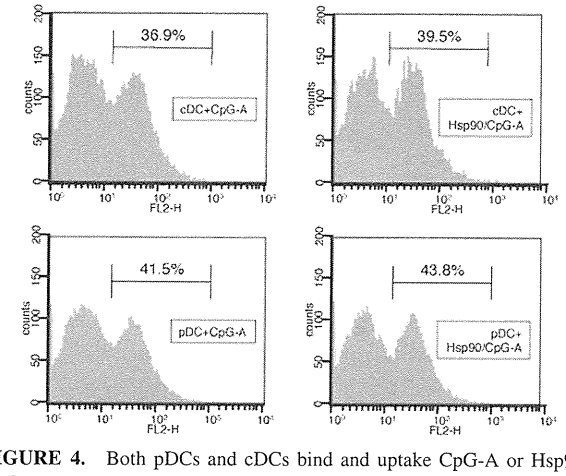


**FIGURE 4.** Both pDCs and cDCs bind and uptake CpG-A or Hsp90–CpG-A complex to similar degrees. Flow cytometric analysis for binding and uptake of Cy5-labeled CpG-A alone (*left panels*) or in complex with Hsp90 (*right panels*) by cDCs (*top panels*) and pDCs (*bottom panels*) after 30 min stimulation. Data are representative of three independent experiments.

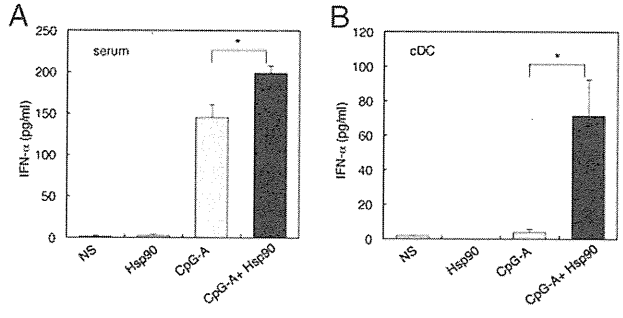


**FIGURE 5.** CpG-A–Hsp90 complex serves as a potent inducer for IFN-α in vivo. CpG-A (50 μg/mouse) or CpG-A–Hsp90 (50 μg/mouse) complex was administered i.p. to C57BL/6 mice 6–10 wk of age. *A*, After 12 h, mouse serum was obtained via cardiac puncture and levels of IFN-α were measured using ELISA. *B*, Mice were then euthanized for spleen removal. cDCs were isolated and cultured for 24 h, and the supernatant was measured for IFN-α production. Data are presented as means + SEM of triplicate wells. Data are representative of three independent experiments. $*p < 0.01$; paired Student *t* test.

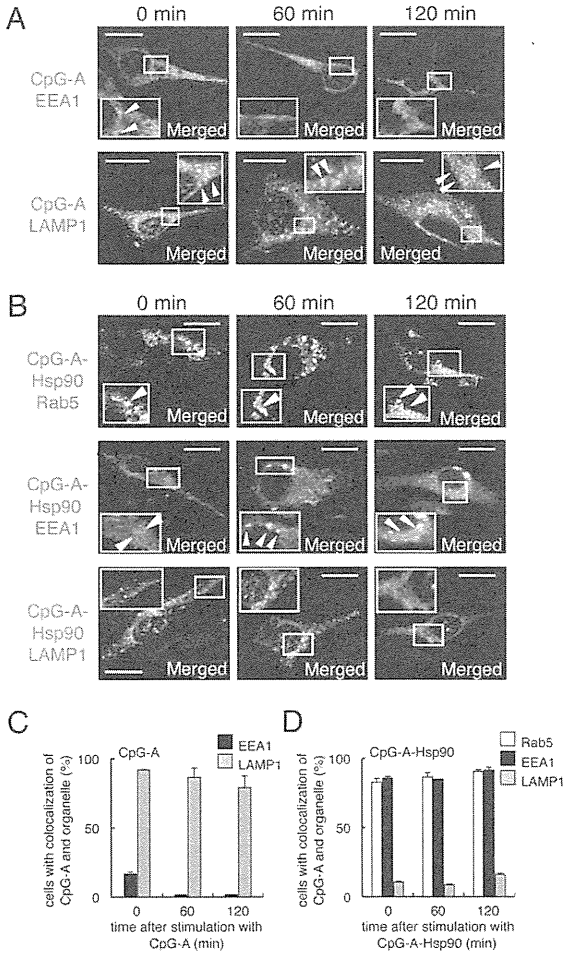


**FIGURE 6.** Hsp90 targets CpG-A to the early endosome for longer periods. Isolated cDCs were pulsed with 3 μM Cy5-labeled CpG-A (*A*) or 3 μM Cy5-labeled CpG-A–Hsp90 complex (*B*) for 30 min. Postincubation with new medium without CpG-A for 0, 60, and 120 min, the cells were fixed, stained, and then visualized by laser confocal microscopy (original magnification ×630). Arrowheads indicate colocalization of CpG-A and each organelle. Bar, 10 μm. Data are representative of three independent experiments. For evaluation of colocalization, a single *z*-plane of one cell was evaluated. For each CpG-A (*C*) or CpG-A–Hsp90 complex (*D*) and organelle combination, a total of 150 cells (50 cells each from three independent experiments) were analyzed.

CpG-A stimulation, which changed to 1.7% and 78.9%, respectively, with the passage of time (Fig. 6*C*). In contrast, the colocalization rates between the Cy5-labeled CpG-A that formed a complex with Hsp90 and Rab5, EEA1, and LAMP1 were 90.6%, 91.5%, and 16.2%, respectively, at 2 h after CpG-A sitimulation (Fig. 6*D*). These data suggested that Hsp90 could target CpG-A to the static early endosome, resulting in efficient TLR9 stimulation for a high amount of IFN-α production by cDCs. Thus, Hsp90 had the ability to retain CpG-ODNs for longer periods in the static early endosome, presumably enabling the selective and continuous activation of early endosomal TLR9 via spatiotemporal targeting of CpG-ODNs.

*Extracellular Hsp90 converts CpG-B into a trigger of IFN-α production by cDCs*

Recent studies have indicated that TLR9 signaling in late endosomes induces DC maturation and TNF-α and IL-6 secretion. We therefore tested whether Hsp90 could convert CpG-B, which was expected to stimulate TLR9 in late endosomes, into a ligand that triggered TLR9 in early endosomes to produce IFN-α. When complexed with Hsp90, CpG-B induced robust IFN-α production from cDCs (Fig. 7*A*) and only low levels of TNF-α and IL-6 as compared with CpG-B alone (Fig. 7*B*, 7*C*). The CpG-B–Hsp90 complex also failed to induce cDC maturation (data not shown). Consistent with these results, the production of TNF-α and IL-6 from cDCs was inhibited when they were stimulated with the CpG-A–Hsp90 complex as compared with CpG-A alone (Supplemental Fig. 4).

*Extracellular Hsp90 enhances the IFN-α production by human pDCs*

In humans, pDCs and B cells express TLR9 (10, 33). We examined whether the CpG-A–Hsp90 complex also induced IFN-α from human DCs as observed in mouse DCs. The production of IFN-α when we stimulated PBMCs of healthy donors with the CpG-A–Hsp90 complex was enhanced when compared with CpG-A alone ($p < 0.05$) (Fig. 8*A*). We observed that PBMC-derived mDCs expressed little TLR9 and that $CD19^+$ B cells expressed TLR9 at a low level (data not shown). Therefore, it was reasonable that there was little IFN-α production by these cells following stimulation with CpG-A or the CpG-A–Hsp90 complex (Fig. 8*B*, 8*C*). In contrast, as pDCs isolated from PBMCs have been shown to produce large amounts of IFN-α, we examined whether Hsp90 could affect the IFN-α production by human pDCs. The CpG-A–Hsp90 complex induced augmented production of IFN-α compared with CpG-A alone (Fig. 8*D*). We therefore concluded that Hsp90-mediated spatiotemporal targeting to static early endosomes of CpG-ODN boosted TLR9 activation and triggered efficient IFN-α induction in mouse pDCs, cDCs, and human pDCs.

*Hsp90 converts self-DNA into a potent trigger of IFN-α induction by human pDCs*

Finally, we determined whether the extracellular Hsp90 enabled human pDCs to sense self-DNA, leading to IFN-α production. Human genomic DNA, which was isolated from healthy volunteers, was unable to induce IFN-α from pDCs. However, we found that self-DNA complexed with Hsp90 could induce IFN-α production from pDCs (Fig. 9). Thus, Hsp90 converted inert self-DNA into an activator of pDCs.

## Discussion

pDCs sense certain viral and microbial infections. In contrast to mDCs, pDCs uniquely express TLR7 and TLR9, intracellular receptors that recognize viral/microbial nucleic acids within endosomal compartments in humans. Together with the constitutive expression of IRF7, TLR7 and TLR9 permit pDCs to mount rapid and robust type I IFN responses to viral/microbial infections. However, pDCs normally do not respond to self-DNA, which may reflect the fact that viral/bacterial DNA sequences contain multiple CpG nucleotides that bind and activate TLR9, whereas mammalian self-DNA contains fewer such motifs, which are most likely masked by methylation. Recent evidence, however, suggests that self-DNA has the potential to trigger TLR9, but may fail to do so because it fails to access the TLR9-containing endolysosomal compartments. One of the mechanisms of this effect is attributed to the fact that DNase easily and rapidly breaks down the extracellular DNA, thereby hampering self-DNA localization into endocytic compartments. In contrast to the human system, murine cDCs, like pDCs, express TLR7 and TLR9.

Two classes of synthetic ODNs containing an unmethylated CpG motif have been classified: CpG-A ODN, which stimulates IFN-α production by pDCs, and CpG-B ODN, which does not. Instead, CpG-B ODN stimulates pDCs to produce IL-6 and TNF-α and induce DC maturation, such as the upregulation of CD80 and